Calculations of Turbulent Flow and Heat Transfer in Periodically Converging-Diverging Channels

by

Ikram-ul-Haq Siddiqui

A Thesis Presented to the

FACULTY OF THE COLLEGE OF GRADUATE STUDIES

KING FAHD UNIVERSITY OF PETROLEUM & MINERALS

DHAHRAN, SAUDI ARABIA

In Partial Fulfillment of the
Requirements for the Degree of

MASTER OF SCIENCE

In

MECHANICAL ENGINEERING

May, 1995

Calculations of Turbulent Flow and Heat Transfer in Periodically Converging-Diverging Channels

BY

Ikram-Ul-Haq Siddique

A Thesis Presented to the

FACULTY OF THE COLLEGE OF GRADUATE STUDIES

KING FAHD UNIVERSITY OF PETROLEUM & MINERALS

DHAHRAN, SAUDI ARABIA

In Partial Fulfillment of the
Requirements for the Degree of

MASTER OF SCIENCE
In
MECHANICAL ENGINEERING

May, 1995

KING FAHD UNIVERSITY OF PETROLEUM AND MINERALS
DHAHRAN, SAUDI ARABIA
COLLEGE OF GRADUATE STUDIES

This thesis, written by

Ikram-Ul-Haq Siddique

under the direction of his Thesis Advisor, and approved by his Thesis committee, has been presented to and accepted by the Dean, College of Graduate Studies, in partial fulfillment of the requirements for the degree of

MASTER OF SCIENCE IN MECHANICAL ENGINEERING

Thesis Committee :

Med Habib

Dr. M.A. Habib (Chairman)

Dr. S.A.M. Said (Co-Chairman)

Dr. H.M. Badr (Member)

Dr. B.S. Yilbas (Member)

Department Chairman (Mech. Engg.)

Dean, College of Graduate Studies

Date: 17-7-95

Dedicated to

my *Parents*

&

my *Brothers* **and** *Sisters*

Acknowledgment

In the name of Allah, Most Gracious, Most Merciful. Read in the name of thy Lord and Cherisher, Who created. Created man from a {*leech-like* } clot. Read and thy Lord is Most Bountiful. He Who taught {the use of} the pen. Taught man that which he knew not. Nay, but man doth transgress all bounds. In that he looketh upon himself as self-sufficient. Verily, to thy Lord is the return {of all}.

(The Holy Quran, Surah 96)

First and foremost, all praise to Allah, *subhanahu-wa-ta'ala*, the Almighty, Who gave me an opportunity, courage and patience to carry out this work. I feel privileged to glorify His name in the sincerest way through this small accomplishment. I seek His mercy, favor, and forgiveness. And I ask Him to accept my little effort. May He, *subhanahu-wa-ta-Aaala*, guide us and the whole humanity to the right path *(Aameen)*.

Acknowledgement is due to King Fahd University of Petroleum & Minerals for providing support to this research work.

I am indebted to my thesis advisor, Dr. Mohamed A. Habib for his help and advice. I acknowledge him for his valuable time, encouragement and guidance especially during the early stages of this work and my M.S studies. Working with him was indeed a learning experience.

I am grateful to my thesis co-advisor, Dr. Syed A.M. Said for his deep interest, constructive criticism and stimulating discussions during the course of this work. Thanks are also due to the my thesis committee member, Dr. Hasan M. Badr and Dr. Bekir S. Yilbas for their comments and critical review of the thesis.

I am thankful to the department chairman, Dr. Mohammad O. Budair and other faculty members for their cooperation.

I am thankful to my fellow graduate students and all my friends on the campus especially Aleem, Asif, Asim, Naweed, Rashid and Shuja who provided a wonderful company.

Last but not the least, thanks are due to the members of my family for their emotional and moral support throughout my academic career. No personal development could ever take place without the proper guidance of parents. This work is dedicated to my parents for taking pains to fulfill my academic pursuits and shaping my personality. They taught me the fundamental concept of life, "Tough times

never last, tough people do". My younger brother Rizwan, deserve special mention for his sacrifices, constant inspiration and guidance. I am grateful to my Father for his support and motivation during the final stages of the work. I acknowledge with gratitude, the affection and encouragement of my sisters (Anjum, Saima, and Fizzah) and brothers (Rizwan and Zubair) that helped me overcome homesickness and concentrate on my work.

Contents

List of Tables

List of Figures

Nomenclature

a	amplitude of sinusoidal wall
A	coefficients in eq. 4.10
C	convective flux
C_p	specific heat
$C_\mu, C_{\varepsilon 1}, C_{\varepsilon 2}$	constants in turbulence model
D	diffusive flux
D_H	channel hydraulic diameter
E'	additional terms in turbulence model
E	roughness parameter (law of the wall)
f_1	coeff. of generation term of ε in turbulence model
f_2	correction function of destruction term of ε in turbulence model
f_μ	damping function for laminar viscosity μ in turbulence model
g_{ij}	metric tensor
G	generation rate of turbulence kinetic energy
h	local convective heat transfer coefficient or scale factor
H	enthalpy
H	height of the channel
$H_i(j)$	metric tensor

J	total flux across the finite difference cell
k	kinetic energy of turbulence
K	thermal conductivity of the fluid
L_c	length of the period or module
m	mass flow rate
Nu	Nusselt number
p	mean static pressure
p'	periodic pressure
P_e	Peclet number
Pr	Prandtl number
ΔP	per-cycle pressure drop
q	local heat flux
r	radius
Re	Reynolds number ($\rho U_m D_H/\mu$)
S	swirl number
S_ϕ	source or sink of variable ϕ
T	absolute temperature
U, V, W or u, v, w	time averaged velocity components
W	width of the channel
x, y	axial coordinate directions

x_i	cartesian coordinate directions
y_p^+	dimensionless distance from the wall

Greek Symbols

$2a/\lambda$	aspect ratio
α, β	constants used in boundary conditions
ε	dissipation rate of turbulence energy
δ	kronecker delta
Γ_ϕ	exchange coefficient for ϕ
κ	Von Karman constant (law of the wall)
λ	wave length of a module
μ	viscosity
∇	gradient/divergence operator
ν	kinematic viscosity
ϕ	general dependent variable
ψ	stream function
ρ	density of the fluid
σ, σ_t	constants in energy equation
$\sigma_k, \sigma_\varepsilon$	constants in turbulence model
τ	shear stress
ξ	transformed orthogonal coordinate

Subscripts

avg	average
b	bulk
e	effective
$exit$	exit
E, N, S, W	values at east,north,south, and west node points
e, n, s, w	values at east,north,south, and west edges of the cell
fd	fully developed
h	hydraulic
i, j, k, l	tensor subscript notation
i	inner wall
m	mean
max	maximum
min	minimum
o	outer wall
P	values of node point P
t	turbulent
w	wall
$1, 2, 3, x$	directions
$*$	guessed values

Abstract

Name: Ikram-Ul-Haq Siddique

Title: Calculations of Turbulent Flow and Heat Transfer in Periodically Converging-Diverging Channels

Major Field: Mechanical Engineering

Date of Degree: May, 1995

A numerical study of flow in a Periodically Converging-Diverging Channel is performed to examine turbulent separated flow and heat transfer characteristics. This geometry has numerous applications in high-performance heat exchanging systems because of its effective influence on heat transfer augmentation. The method is based on the fully conserved control-volume representation of fully elliptic Navier-Stokes, and Energy equations in body-fitted orthogonal curvilinear coordinate system. Turbulence is simulated via two-equation ($k-\varepsilon$) model.

The presented results consist of computed velocity and streamline distributions, the kinetic energy of turbulence, pressure drop, friction factor, and local, average and maximum Nusselt number distribution. Systematic variations are made in Reynolds number (40,000 to 100,000) and the aspect ratio ($2a/\lambda$=0.27 and 0.34). The study is further extended to flows with different ranges of inlet swirl. The results are compared with the different available experimental data and show that the method with the utilized turbulence closure model and the discretization scheme reproduce the essential features of various channel heat transfer and fluid flow effects observed in experiments.

Master of Science Degree
Department of Mechanical Engineering
King Fahd University of Petroleum and Minerals
Dhahran, Saudi Arabia
May, 1995

ملخص

الإسم : إكرام الحق صديقي

الموضوع : حساب الإنسياب المضطرب وانتقال الحرارة داخل القنوات المتسعة والمنضغطة دوريا

التخصص : هندسة ميكانيكية

تاريخ الشهادة : مايو ١٩٩٥م ٠

هذا البحث يشتمل على دراسة عددية للسريان المضطرب وانتقال الحرارة داخل القنوات المتسعة والمنضغطة دوريا ٠ إن لهذا الشكل تطبيقات عديدة في ناقلات الحرارة العالية الجودة لأن الشكل له تأثير فعال في نقل الحرارة ٠ تعتمد الطريقة على إستخدام طريقة الحجم المحدد لحل معادلات نفير - ستوكز والطاقة باستخدام إحداثي مائل ٠ مثل إضطراب السائل باستخدام التمثيل ($k-\varepsilon$) ثنائي المعادلات ٠

النتائج الموجودة في البحث تتكون من حسابات السرعة وتوزيع متوازيات السرعة والطاقة الحركية في الإضطراب وانخفاض الضغط ومعامل الإحتكاك ورقم نوسيلت المحلي والمعدل ٠ وقد تم عمل تغيير منظم في رقم رينولدز من (٤٠ر٠٠٠ - ١٠٠ر٠٠٠) وتغيير نسبة الطول إلى العرض من ٢٧ر - ٣٤ر٠

تم تمديد الدراسة إلى درجات مختلفة من التدويم عند المدخل ٠ وقد تم مقارنة النتائج مع المتوفر من النتائج التجريبية والتي توضح أن النموذج المستخدم يطابق النتائج المستخرجة لإنتقال الحرارة والسريان في الأشكال المذكورة من الواقع العملي ٠

درجة الماجستير في العلوم
قسم الهندسة الميكانيكية
جامعة الملك فهد للبترول والمعادن
الظهران ، المملكة العربية السعودية
مايو - ١٩٩٥م ٠

Chapter 1

Introduction

1.1 Fluid Dynamics

The establishment of the science of fluid dynamics and the practical applications of that science has been under way since the time of Newton. The theoretical development of fluid dynamics focuses on the construction and solution of the different categories of fluid dynamics and the study of various approximations to its equations.

The governing equations for Newtonian fluid dynamics, the Navier-Stokes equations, have been known for 150 years, but these equations are non-linear and are not amenable to closed-form solution for general geometry. The steady improvement in the speed of computers and the memory size since 1950's has led to the emergence of computational fluid dynamics (CFD). This branch of fluid dynamics complements experimental and theoretical fluid dynamics by providing an alternate cost-effective

means of simulating real flows. As such it offers the means of testing theoretical advances for conditions unavailable experimentally. CFD also provides the convenience of being able to switch off specific terms in the governing equations. This permits the testing of theoretical models and, inverting the connection. suggests new paths for theoretical exploration. Five major advantage of CFD compared with experimental fluid dynamics are:

- Lead time in design and development reduce significantly.
- CFD can simulate flow conditions non-reproducible in experimental model test.
- CFD provides more detailed and comprehensive information.
- CFD is increasingly more cost-effective than wind-tunnel testing.

On the other hand, computational methods also have limitations: among these are computer storage, speed and cost. Other limitations arise due to inability to understand certain complex flow phenomena, incorrect mathematical model, truncation errors, improper boundary conditions, approximations and assumptions, that are made to simplify the problem, and to increase the computing efficiency.

1.1.1 How to Formulate a Problem

Some of the basic steps required to solve flow problems (see Fig. 1.1) are:

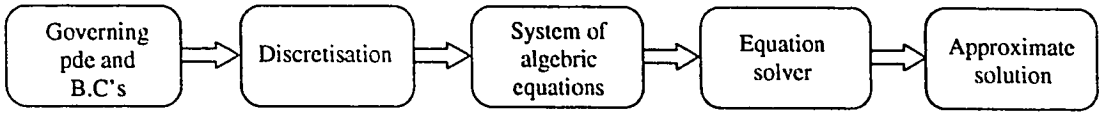

Figure 1.1: Overview of the computational procedure

Suitable Mathematical Model

The first step is to develop a mathematical model for a specific problem with governing equations and the appropriate boundary and initial conditions specifying the flow.

Computational Techniques

The process of obtaining the computational solution is done by replacing the governing Partial Differential Equations (PDE or pde) and auxiliary (boundary and initial) conditions, with discrete system of algebraic equations. The algebraic equations linked together values of dependent variables at adjacent grid points. The process of converting the continuous governing equations into discrete system of algebraic equations is known as discretization.

Solution of a CFD Problem

The algebraic equations produced by discretization can now be solved by appropriate methods, that are discussed later. The next stage is to develop algorithm, use to solve the equations by using computer programming.

1.1.2 Computers and CFD

The evolution of numerical methods, especially finite-difference methods for solving ordinary and PDE began at about the turn of this century, with the advent of automatic digital computer in late 1930's. But explosion in computational activity began in 1960's, with availability of high-speed digital computers.

Traditionally, both experimental and theoretical methods have been used for the development and designing of equipments involving fluid flow and convective heat transfer. With the advent of digital computers, a third method, the numerical approach, has become available.

The future trends for computer speed and memory capacity are encouraging, and are expected to be adequate for predictions of unsteady, viscous, turbulent and compressible flow.

1.2 Turbulence and CFD

From classical point of view, turbulent fluid motion is an irregular condition of flow in which the various quantities (velocity, pressure, concentration, temperature, etc.) show a random variation with time and space coordinates. Some characteristics of turbulence are:

1) Irregularity - The flow is so complicated and irregular that it can neither be followed, nor can be described completely.

2) Three-Dimensionability - Turbulence is always three-dimensional, even when the mean flow is predominantly one or two-dimensional. Flow fluctuations always have components in all three directions.

3) Diffusivity - The rapid mixing of momentum, heat, and mass is a typical feature of turbulent flows.

4) Dissipation - The kinetic energy of turbulent motion is dissipated into heat under the influence of viscosity. The energy supplied to turbulence must come from the mean flow, by the interaction of shear stresses and velocity gradients.

5) Others - The fluid can still be considered as a continuum. Turbulence is a fluid flow feature that occurs at high Reynolds number and is not a property of the particular fluid itself.

Turbulence originates primarily from instabilities in the flow, also commonly associated with high Reynolds number. The most common source is the shear flow instability. Once initiated, turbulence can not maintain itself, but depends on its flow environment to provide kinetic energy, called as *kinetic energy of turbulence.*

With the use of computers, in the modern CFD, definition of "Turbulence" is simply all the phenomena due to the irregular motion that occurs at scale below those resolvable on the grid employed for computational purposes. One of the major challenge to turbulent CFD is:

Physical Complexity

CFD, particularly in engineering, is at the stage of development where problems involving complex geometries contain separated flow field, called recirculation region. These regions are characterized by strong streamline curvatures, complex eddy structures and high turbulence intensities associated with high heat transfer rates and pressure losses. Consequently, when dealing with separated flows in theory, detailed knowledge of the underlying physics is required. It is therefore appropriate to carry out investigations concerning separated flows on flow configurations with simple geometric boundary conditions. Sometimes experiments are necessary to study the mean flow field (including the influence of the wall) as well as the determination of turbulence modeling. By combining experiments and computation, possibilities of comparing performance of turbulence model used in numerical procedure are offered on one hand, while on the other, experimentally determined correlation quantities are provided which are used as input parameter in calculation procedures.

1.3 Some Terminologies in Numerical Techniques

1.3.1 Convergence

Solution of the algebraic equations which approximates a given partial differential equation (pde) is said to be convergent if the approximate solution approaches the exact solution of the pde for each value of the independent variable, as the grid spacing tends to zero.

1.3.2 Consistency

System of algebraic equations generated by the discretization process is said to be consistent with the original partial differential equation if, in the limit that the grid spacing tends to zero, the system of algebraic equation is equivalent to the PDE at each grid point.

1.3.3 Stability

This is the tendency for any spontaneous perturbation in solution of the system of algebraic equation to decay.

1.3.4 Truncation Error

Converting the governing differential equations into an equivalent system of algebraic equations, introduces some error. These errors are simply truncated to provide the

approximate translation, and accordingly they are called as truncation error.

1.3.5 Solution Accuracy

Accuracy means, how closely the algebraic equation agrees with partial differential equation. If the grid spacings are sufficiently small, and the initial and boundary conditions are sufficiently smooth, truncation error will usually coincide with the order of the solution error. Refining the grid will very often produce a superior accuracy for the higher-order scheme but at an absolute accuracy level is far higher.

1.4 Turbulence Models

Direct numerical simulations of turbulent flows has been very useful for revealing many interesting phenomena. The governing equations for turbulent flows are in general, highly non-linear and the behavior of these differential equations are not yet well understood.

The simulations themselves are restricted at present to relatively simple geometric regions due to computer limitations, so most calculations for practical configurations are being made through Reynolds-averaged equations of motion with the aid of turbulence modelling.

Turbulence models are classified by the number of transport equations used for turbulence quantities.

1.4.1 Zero-equation Model

Models using only the pde's for the velocity field, and none for turbulence transport equation.

1.4.2 One-equation Model

Models involving one pde relating to a turbulence velocity scale, in addition to the mean-flow pde's.

1.4.3 Two-equation Model

Models using an additional pde related to turbulence length scale (e.g $k-\varepsilon$ model).

1.4.4 Reynolds Stress-equation Model

Models involving pde's for all components of the Reynolds stress tensor and in general, for a length scale as well.

1.5 k-ε Turbulence Model

$k-\varepsilon$ turbulence model consists of k and ε-equations, where k is the turbulent kinetic energy and ε is the isotropic dissipation rate of the turbulent kinetic energy. This model is selected, because it has been tested most widely and successfully to many different problems. Its predictive capabilities for shear-layer flows and also for

confined recirculating flows are well established. A large number of flows have been predicted with the same set of empirical constants [1].

$k-\varepsilon$ turbulence models however do not adequately predict separated flows and heat transfer. Near the reattachment points, heat transfer affected strongly by separation, as the separation increases rapidly and then decays slower than those of ordinary boundary layer flows. This is because of two dimensional factors in the near wall region. One is the local turbulent Reynolds number effect; the laminar viscosity became more important as flow approaches the wall. Another factor close to the wall is the damping of the turbulent fluctuations in the direction normal to the wall. To alleviate these problems, the high Reynolds number turbulence model uses a wall function which connects the surface boundary to a point in the fully turbulent region [2].

In the near wall region fine grids are needed as the heat transfer rate on the wall is very sensitive to the grid geometry because the main temperature difference (upto 50%) is located in the thin near-wall region and the heat must transfer through the viscous sublayer by molecular diffusion. It is difficult to predict adequately the heat transfer rates along the wall even with a satisfactory prediction of the flow field. Unfortunately turbulence model seems to predict heat transfer rates that are too high in the reattachment region after separation. Inside the recirculation zone, the velocities are low, yet the level of turbulent kinetic energy is relatively high. This results from diffusion/transport from the bordering shear layer, where

high turbulence is generated. However, the dissipation of turbulent kinetic energy is small in this zone because of large eddy motions rather than small eddy motions. $k-\varepsilon$ model either neglects the transport of the individual turbulent stresses, or accounts for them only in a rather approximate manner.

Despite of the above mentioned draw-backs, the $k-\varepsilon$ model has been applied successfully to many two-dimensional wall boundary layers, duct flows, free shear flows, recirculating flows, and to three-dimensional wall-boundary layers, confined flows and jets [1].

1.6 Flow Through Periodically Converging-Diverging Channel

1.6.1 The Flow Field

Fluid flow through periodically converging-diverging channel in streamwise direction, shown in Fig. 1.2, differs fundamentally from that of conventional constant area channels.

The periodic contraction and enlargement of the channel cross-sectional area, gave rise to appreciable transverse motions that cause fluid mixing and increase the heat transfer. It is because of this geometry that flow is unable to follow the contours of channel and thus, zones of separation and recirculations appear. The presence of

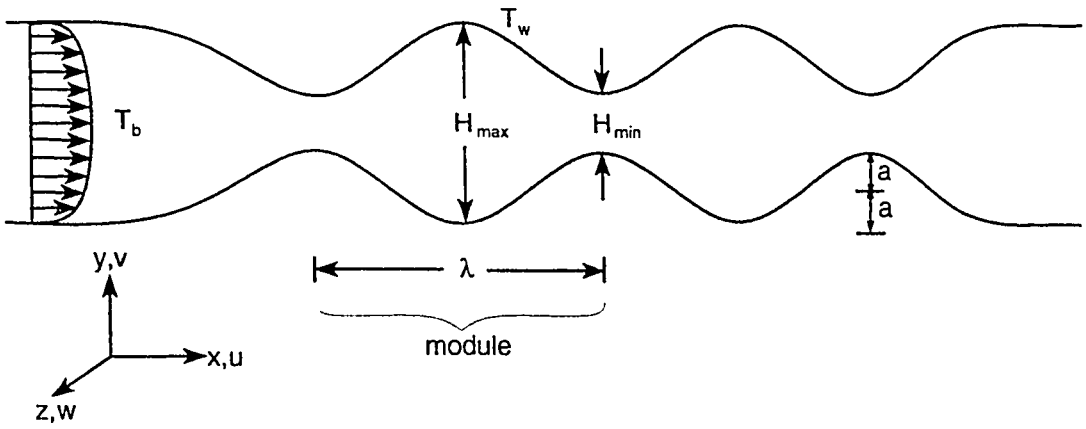

Figure 1.2: Geometry of symmetric sinusoidal converging-diverging channel

these zones further increases the mixing, resulting in higher heat transfer coefficient than that of corresponding smooth channel.

1.6.2 Turbulent Flow

Turbulent flow in converging-diverging channel induces complex flow phenomena which have a profound influence on heat and mass transfer. Complex geometry which is a consequence of the waviness of the wall, centrifugal forces are setup that may induce secondary flow superimposed on the main flow [3]. With the increase of Reynolds number complexity increases, thus making measurements of local heat fluxes and temperatures needed to determine the distribution of the local heat transfer coefficient on the corrugated walls, are very difficult to perform.

Converging-diverging geometry encompasses with accelerating or decelerating flow, separation, reattachment, recirculation and alternating pressure gradient that are not encountered in conventional ducts, such as circular and annular tubes, and straight rectangular channels.

1.6.3 Periodic Fully Developed Flow Regime

The fluid flow encounters flow passages with periodically varying cross section, results in periodic flow. Once flow became periodically fully developed, flow field repeats itself at corresponding axial stations in successive cycles (i.e similar velocity distribution in each module). Furthermore, in such a regime, the pressures of

cyclically corresponding locations decrease linearly in the downstream direction [4]. To obtain final results, periodicity is assumed so that solution is obtained only for a single module (i.e sixth module).

1.6.4 Applications

Recent advances in technology motivates the development of compact heat transfer surfaces in engineering community by the necessity to reduce the size and weight of heat exchange devices such as those encountered in electronic cooling, spacecraft, airconditioning, automobiles, aircrafts, medical and natural applications, etc.

The symmetrical converging-diverging channel is one of the several devices employed for enhancing the heat and mass transfer efficiency of the industrial transport processes. They find good usage in compact heat transfer surfaces, cooling of micro-electronics (in highly efficient heat exchangers) and high-efficiency membrane oxygenator (in which blood is separated from oxygen by microporous membrane and streams in pulsatile flow state through converging-diverging channel constructed by the membrane). The enhancement of oxygen transfer is attributed to convective mixing with unsteady flow separation, induced by oscillating the blood flow itself [5].

The study of the flow through periodically converging-diverging channel is of importance as it would help to understand the flow of fluids in porous media, as in the case with seepage of contaminants into ground water, enhanced oil recovery, flow

of biological fluids through the body, etc. Fluids in porous media move through a tortuous channel. As a result, the flow converges and diverges out of a constriction in the media (i.e the fluid element is being stretched or compressed). Capillary tube models fail to capture this feature; sinusoidal converging-diverging channels on the other hand are sufficiently realistic to include the most important aspects of the flow. There are numerous other problems in engineering where the flow of fluids occurs through torturous paths. Such flows are commonly encountered in polymer processing, flow through porous media, flow of biological fluids such as blood, flow of polymer fluids through fiber networks, etc [6]. Such flows cause enhancement in heat and mass transfer mainly attributed to very well mixed flow.

Viscous fluid flow pasts wavy boundary has some other examples also, like, generation of water waves by wind, evolution of sand-dunes in deserts, melting of ice covers on rivers, formation of sedimentary ripples in river channels, transpiration cooling of re-entry vehicles and rocket boosters, cross-hatching on ablative surfaces, film vaporization in combustion chambers and possibly drag reduction.

1.6.5 Geometry of Periodically Converging-Diverging Channel

The geometry shown in Fig. 1.2 consists of a succession of sinusoidally converging and diverging sections, placed end to end. Each cycle consists of a diverging section

and a converging section, hereafter, be reffered to as a module. The geometry of the channel can be described by the cycle length (or period length), λ, maximum height of the channel, H_{max}, width of the channel in spanwise z-direction, W, and by its amplitude, a. Geometry can also be specified by the aspect ratio, $2a/\lambda$.

To have flow fully developed, the conditions of the flow upstream and the number of waves must be considered. In either case, for wave amplitude greater than some critical value at any Reynolds number, the flow involves multiple regions of separations and reattachments. Description of turbulent flow past a wavy surface involves a number of challenges. In addition to the effects of the alternating favorable and adverse pressure gradient and convex and concave surface curvatures on the turbulence, it is difficult to predict the separation and reattachment points.

The selection of this geometry is because of the reason that it has been studied rather extensively over a number of years in a series of experiments conducted by Hanaratty and his students as mentioned by Patel et al. [7], and shown in Table 1.1.

1.7 The Scope of Present Work

The objective of the present study is to investigate the flow characteristics, turbulence kinetic energy, pressure drop, friction factor, heat transfer, and swirl flow characteristics in sinusoidally varying converging-diverging walled channel by sys-

References	Measurements Made	Re	$2a/\lambda$	Flow Features Observed
Zilker et al. (1977)	wall pressure, wall shear,	6,000-64,000	0.0125 0.03125	linear shear stress responce linear shear stress responce
Zilker et al. (1979)	mean velocity, turbulent velocity, flow visualizations		0.05 0.125 0.2	instantaneous flow reversal seprated flow seprated flow
Thorsness et al. (1978)	wall shear mean velocity	11,000 64,000	0.0114 0.0125	linear shear stress responce linear shear stress responce
Buckles et al. (1984)	mean and fluctuating velocities and wall pressure	24,000	0.02	seprated flow
Abrams et al. (1981,1986)	mean and fluctuating wall shear	11,940 245,000	0.014	linear shear stress responce
Frederick et al. (1986)	mean and fluctuating velocities	12,800 77,600	0.03125 0.05	linear shear stress responce nonlinear stress responce
Kuzan (1986)	wall pressure, mean and fluctuating velocities, flow visualization	96,000 17,000 8,160	0.125 0.05 0.20	instantaneous flow reversal instantaneous flow reversal seprated flow

Table 1.1: Summary of the Experiments of Hanaratty et al. [7]

tematically varying Reynolds number.

The study is conducted at the sixth module, which is sufficiently far downstream where entrance effects are negligible and, therefore, periodic fully developed flow field and heat transfer conditions are obtained. The periodic, fully developed concept, introduced by Patankar et al. [8], is used to solve the steady state problem. The specific aim of this work is to investigate the performance of rectangular, sinusoidally varying converging-diverging walled channel with periodic fully developed turbulent flow field, variation in velocities and Nusselt number, and the turbulence characteristics in the near-wall region which is responsible for the heat transfer, with variations in the amplitude and Reynolds number.

Calculations are presented in chapter 5 for the conditions under which separated flow exists (the extent of the separated region). As the size and intensity of this recirculating flows are expected to influence the rate of heat transfer. effects due to swirl are also considered, for which axisymmetric converging-diverging geometry is used.

For numerical calculations, steady state, two-dimensional, axisymmetric form of continuity, time-averaged Navier-Stokes and energy equations are used along with a turbulence model. In particular, the present analysis, for a flow with separation and reattachment, requires a two-equation model using turbulent kinetic energy and a turbulence length scale. The solution domain is obtained by generating orthogonal curvilinear grid in stream-wise and cross-stream-wise nodes as curvilinear grid that

coincides with the duct boundaries. Finally, solution is performed numerically using modified version of TEACH [9].

Chapter 2

Literature Review

2.1 General Fluid Flow and Heat Transfer

In recent years, computational heat transfer has emerged as a new field, which promises to have significant impact on research, design, and education. The purpose of this chapter is to review some of the recent developments in this field.

Fletcher provide various techniques and formulations alongwith programs, examples, and problems, for various branches of CFD [10, 11]. Abbot and Basco encompasses the definitions, methods and models used in CFD [12]. Patankar describes the different numerical techniques and methods in a very simple way [13].

Recent developments in computational heat transfer and fluid flow were reviewed by Patankar [14]. Different solution algorithms, grid generation techniques, models, and educational aspects were also discussed. Patankar has given an overview of the

techniques of obtaining numerical solution of heat transfer and fluid flow problems [15]. In another article he discussed calculation of elliptic and parabolic flows, by using implicit finite-difference method [16].

2.2 Coordinate System

The rectangular cartesian coordinate system has been used in many previous investigations for separated flows and is quite laborious and inaccurate [17]. Therefore the best solution is to use orthogonal curvilinear coordinates where the solution domain is coincident with the flow boundaries [17, 18, 19, 20, 21, 22]. Presently most of the research work is done by using non-orthogonal curvilinear coordinates [23, 24, 25]. Flow in arbitrary complex geometries is studied by Karol et al.[26]. Computation of recirculating turbulent flow in complex geometries by using full multigrid, curvilinear coordinates is studied by Shyy et al. [27].

2.3 Turbulence Model

To analyze the turbulent flow in separated regions, and to show the instabilities of flow in a symmetric geometry by numerical method, turbulence models are required.

$k - \varepsilon$ two-equation model is the one applied most widely for the flow contains separation, reattachments and recirculation regions [1, 17, 19, 20, 21, 27, 28, 29, 30, 31]. A good example of evaluating the $k - \varepsilon$ model with other turbulence models

is done by Hanaratty et al. [32]. Another comparison between one-equation and two-equation ($k-\varepsilon$) model with experimental confirmation is made by Rodi et al. [33].

Detailed simulation of two-dimensional turbulent flow by using $k-\varepsilon$ model is done by Elkaim et al. [34]. Low-Reynolds-number $k-\varepsilon$ model is revised by Cho et al. [2].

Two-equation $k-kl$ model is used in two-dimensional periodic flow by Izumi et al. [35]. Amano et al. uses Reynolds-Stress Model (RSM) for the evaluation of turbulence quantities in periodically corrugated wall channel [36]. Number of different mathematical turbulence models were given by Rodi [1], and Launder and Spalding [37].

2.4 Solution Methods

There are number of different numerical methods available for the solution of incompressible Navier-Stokes equations. Among them the most popular one is the SIMPLE (*Semi-Implicit Method for Pressure-Linked Equations*) algorithm. SIMPLE algorithm has been used for different flow and geometric conditions [13, 16, 17, 24, 38]. The detailed procedure is also discussed by Gosman [9]. Patankar studied different methods applied in numerical heat transfer including SIMPLE and SIMPLER [14]. The actual SIMPLE method used so called HYBRID scheme for discretization of

the combined convection and diffusion fluxes. The scheme simultaneously possesses unconditional stability, high computational efficiency and algorithmic simplicity [39].

SIMPLER, a revised form of SIMPLE algorithm in which an extra equation is solved for the evaluation of pressure, and is typically 50% more efficient and it converges under conditions in which the other methods diverge [11]. However, ocassionally rather unexpected and surprising results are obtained [14]. This method has been used by many researchers successfully [2, 7, 40, 41, 42, 43]. Another variant of SIMPLE is, SIMPLEC, which uses underrelaxations for the momentum and pressure correction, used by Grag et al. [44]. SIMPLEST is the enhanced form of SIMPLE, which has explicit treatment of convection and implicit treatment of diffusion in momentum equation [14].

Among other methods, one is QUICK (*Quadratic Upstream Interpolation for Convective Kinematics*). It is a multilevel-multigrid technique for recirculating flow [14, 11]. Shin apply QUICK for two-dimensional turbulent flow [21]. QUICK scheme is divergent on a very distorted mesh and generally requires more iterations when it is convergent.

Guzman and Amon used implicit Euler backward and Crank-Nicolson schemes [45], which is also used by Amon et al. for studying self-sustained oscillatory flow in communicating channels [46].

Nishimura et al. uses Galerkin finite element method for numerical analysis of pulsatile flow in a wavy channel [5]. Upward finite difference scheme is applied by

Kang and Chang , for the solution of flow with turbulence promoters [47]. Benjamin uses asymptotic approximation of integral to study the shearing flow over a wavy boundary [22].

2.5 The TEACH Program

Wang discussed the importance of numerical grid generation in computer simulation of fluid flow and heat transfer in complex geometries for both finite difference and finite element methods [48].

For the solution of finite-difference form of partial differential equations there are different computer programs available, TEACH-family is among one of them, written in FORTRAN 77, is very general and adaptable. By performing minor modifications, it can be used to simulate vastly different problems of heat transfer and fluid flow [9]. TEACH program has been used for range of two-dimensional recirculating flows [28]. Chieng and Launder used TEACH-2E for the solution of turbulent flow and heat transfer in the separated flow, created by an abrupt pipe expansion [30]. Amano performed numerical study of turbulent flow with abrupt expansion, used TEACH [31]. It is also used successfully by the others to study turbulent flows in different geometries [9, 17, 20].

2.6 Periodic Fully Developed Flow Regime

The concept of fully developed periodic flow and heat transfer in channels whose cross-sectional area varies periodically in streamwise direction is firstly given by Patankar et al. [8]. This concept of periodic fully developed flow has been applied on numerous geometries of ducts with periodically varying flow cross-sections. For example flow through circular tubes with longitudinal fins interrupted in streamwise direction by arranging either in staggered or an in-line manner is studied by Kelkar and Patankar [41]. The study of two-dimensional finned passages formed by two parallel plates to which fins are attached in staggered fashion, shows that it contains identical geometric modules [40, 42]. The flow attains periodic fully developed regime, in which the velocity field repeats itself from module to module, and the flow become periodic after 3 to 5 modules from the entrance region, as reported by Kelkar et al. [40].

Asako and Faghri applied this concept to predict fully developed flow in corrugated duct, in which the periodic fully developed velocity field repeats itself at corresponding axial stations in successive cycles [24, 25]. Furthermore, in such a regime, the pressures of cyclically corresponding locations decreases linearly in the downstream direction.

Other cases of flow in periodically varying cross-sectional area with periodic boundary conditions are reported by; Izumi at al. [35], Ramadhyani [43]. Amon et

al. [46], and Sparrow et al. [49, 50].

2.7 Methods of Heat Transfer Augmentation

The development in heat transfer augmentation has received much attention in the engineering community. Patankar studied how circumferential distribution of the wall heat flux affects the forced/natural convection flow and heat transfer in a horizontal tube, with two different heating conditions [51]. Effects on heat transfer in a circular tube with longitudinal fins is studied by Kelkar et al. and reported significant increase in heat transfer as compared to the tube without fins [41].

Turbulent heat transfer in a downstream expansion is studied quite a lot with different geometries [17, 30. 31]. Some studies were also performed on heat transfer in expanding duct with and without swirl [52, 20].

Patankar et al. studies heat transfer in ducts with periodically fully developed flow and concluded that the velocity components are periodic and the pressure also reduces periodically [8]. There are many other examples of increase in heat and mass transfer due to turbulence promoters (zigzag-type, cavity-type, grooved-type, interrupting plates-type, staggered ribs-type and fin-type) [40, 42, 46, 47, 53, 54].

2.8 Periodically Converging-Diverging Channels

2.8.1 Numerical Studies

The development of high-performance thermal system has stimulated the interest in heat transfer by using augmentation techniques. A passive method of augmentation is the utilization of rough surfaces that promotes mixing rather than to increase heat transfer area [45]. Among different promoter surfaces, channel with periodically varying cross-section is studied and tested by many others.

Benjamin studied theoretically the flow bounded by simple-harmonic wavy surface, and calculated the normal and tangential stresses on the boundary [22]. The prediction of shear stress and pressure variation in a channel with sinusoidal bottom wall is studied by Hanaratty et al. [32]. Izumi et al. investigated corrugated walled channel bent many times with different angles, and analyzed fluid flow and heat transfer characteristics under the constant wall heat flux condition for the laminar (Re=0 to 2400) and turbulent (Re=40,000) flows [35]. Amano performed a study on hydrodynamic and heat transfer characteristics in periodically corrugated walled channel at a 90 degree bend, for both laminar and turbulent flows, with Reynolds number range varying from 10 to 25,000 [29]. In another paper, the continuation of above is studied with fin plates inserted in the flow passages in order to investigate the local flow characteristic variations for Re=2000 to 20,000 [36]. Izumi studies channel with many bends. to measure the heat transfer characteristics [55].

Ramadhyani presents computational method for the determination of the flow velocities and temperature distributions in a wavy fin passage of the repeating geometric pattern in the streamwise direction, for Re=130 to 560 [43]. Asako et al. evaluated the performance of corrugated duct, the pressure drops, friction factors, and Nusselt number for the range of Reynolds number between 100 and 1.500 [24]. Results were compared with the corresponding values for unidirectional duct under three different constraints. In another paper Asako et al. studied the performance of corrugated duct with rounded corners (Re=100 to 1000) and compared with straight duct and to a duct with sharp corners under three different constraints: fixed pumping power, fixed pressure drop, and fixed mass flow and reported either increase or decrease in heat transfer depending upon the specific conditions [38]. Patel et al. examined the steady turbulent flow in two-dimensional rectangular channel with fixed sinusoidally wavy wall at the bottom, with different amplitude-to-wavelength ratio for Reynolds number range from 8,160 and 12,800 [7].

Periodically converging-diverging wall channel has been investigated by Faghri and Asako at low Reynolds number (Re=90 to 1635), for three different aspect ratios (H_{max}/H_{min}=1.2,1.5 and 2.0) [25]. Results shows moderate enhancement in Nusselt number as compared with corresponding value for straight duct, and reported increase in pressure drop as the angle or Reynolds number increases. Phan-Thien and Khan Studied the fluid flowing through a sinusoidally corrugated tube and describes a numerical method which is based on a boundary element method for solution of

the problem [56]. They study velocity distribution, and contours for velocity and streamlines. For the confirmation of their results they used experimental data on the fluid flow through a sinusoidally corrugated tube.

Numerical work for laminar flow (Re=100 to 1000) of various taper angles of converging-diverging sections, for two length-diameter ratios of the periodic geometry was carried out by Sparrow and Prata and compared Nusselt number with straight duct [50]. Nishimura et al. studied flow in periodically varying converging-diverging cross-sections with Reynolds number range from 250 to 5000, with geometry similar to that of Oxford membrane blood oxygenator, and analyzed the mass transfer characteristics [5, 57].

Sinusoidally curved converging-diverging channel with periodic flow was presented by Grag and Maji for the Reynolds number ranging from 100 to 500, and wall amplitude-to-pitch ratio varying from 0.1 to 0.25 [44]. Detailed results of U and V (velocity profiles), enthalpy profiles, pressure drop and variation of Nusselt number were also given.

Flow patterns and forced convective heat transfer is described by Guzman and Amon in periodically varying symmetric converging-diverging rectangular channel with sinusoidal upper and lower wall, for Reynolds number ranging from 20 to 500 [45]. These numerical simulations resolves time-dependent oscillatory flow, and investigate the early transition process through a stress of bifurcations from laminar to chaotic flow, establish the flow conditions under which the periodic flow loses

stability leading to chaotic state prior to the fully-turbulent flow.

2.8.2 Experimental Work

The separation phenomena in internal flows caused by sudden changes in flow geometry is very well known. The importance of such flows to engineering equipment has been stressed in many publications.

Armaly and Drust perform experiment on internal flow with separation regions by measurements of velocity over a wide Reynolds number range [58]. Experiments on a duct of rectangular cross-section with parallel walls and having interrupted plates in between them. is conducted by Amon et al. to investigate the flow fields and thermal phenomena, and observes significant enhancement in mixing [46]. Kang and Chang observed flow separation by visualization, for three different types of promoters, to find the streamline distributions and the eddy lengths in order to validate the results of numerical analysis [47].

Experiments were carried out to determine the local and average heat transfer characteristics for flow in a in-phase corrugated wall channel by Goldstein and Sparrow [59]. The experiments demonstrated the existence of a variety of complex transfer processes and related fluid flow phenomena, including secondary flows and associated spanwise mass transfer variations. O'Brien and Sparrow performed experiments to determine forced convection heat-transfer coefficients and friction factors for flow in a in-phase corrugated duct, with corrugation angle of 30 degrees,

for Reynolds number ranging from 1500 to 25,000 [60]. Flow visualization revealed a highly complex flow patterns, including large zones of recirculations adjacent to the rearward-facing corrugation facet. The enhancement of heat transfer was compared to a conventional parallel-plate and was found to be increased by the factor of two [55]. Sparrow and Comb determined experimentally the heat transfer, pressure drop and patterns of fluid flow, for water flow in an in-phase corrugated-wall duct for Reynolds number varying from 2000 to 27,000 [61]. Consideration was given to the effects of varying the spacing between the walls and of different fluid flow inlet conditions. Oyakawa et al. investigated the effects on heat transfer and fluid flow by the using sinusoidally varying in-phase corrugated channel [62]. Zilker et al. measured the shear-stress variations and velocity profiles in a channel with sinusoidally varying wavy wall bottom, for turbulent flow with height-to-weight ratios of 0.0312 and 0.05 [63, 64].

The effects of passive flow destabilization on augmenting of the heat transfer/pumping power performance of rectangular channel with converging-diverging grooved wall at the bottom, is studied experimentally by Greiner et al. for the Reynolds number range 300 to 5000 [65]. Ektesabi et al. performed experiments to determine flow and heat transfer characteristics, and friction factor for turbulent flow in wavy sinusoidally varying bottom walled channel, with Reynolds number ranging from 300 to 40,000 [66]. Flow visualization revealed that the periodic change in the size of the recirculation zone was accompanied by a sweep and burst of large-scale

vortices.

Sano and Asako investigated the effects of pressure gradient on fluid flow and heat transfer in duct with bottom wall, smooth plate and top wall corrugated [67]. The specific aim was to study turbulence characteristics in the near-wall region which is responsible for the heat transfer. The relationship between the heat transfer and fluid flow was also examined, with variations in the taper angle of diverging-converging duct and Reynolds number. Ali et al. performed experiments to study heat transfer in the entrance region of corrugated channels [68]. Two channel spacings were examined for single corrugation angle of 20 degree, and flow rate varied over the range of Re=150 to 4000. Increase in Nusselt number of about 140% over the parallel-plate channel was reported and performance evaluations under the criteria of equal mass flow rate, equal pumping power, in comparison with the parallel plate channel was also given. Molki and Yuen conducted experiments to determine the per-cycle heat transfer coefficient for turbulent flow in a isothermal, corrugated-wall duct with variable inter-wall spacing [69]. The focus of the study was on two regions of the duct: the combined thermal-hydraulic entrance region and the periodic fully developed region.

A comprehensive experimental study was performed to determine entrance region and developed heat transfer coefficients, pressure distributions and friction factors, and patterns of fluid flow in periodically converging-diverging tube was performed by Mendes and Sparrow, with an overall range of Reynolds number for the experiments

extending from 6000 to 70.000 [70]. Systematic variations were made in Reynolds number, the taper angle of converging-diverging modules and the aspect ratio, and reported large enhancements of heat transfer coefficient (30 to 60 %), accompanying with large pressure drops.

Narayan et al. studied transport phenomena in diverging-converging geometries [71]. Stephanoff studied shear layer oscillations in a diverging-converging multi-cavity channel for Reynolds number range from 5 to 30 [72]. Similar studies on periodic converging-diverging channel to investigate wall shear-stress, pressure drop, mass transfer and flow characteristics were performed by Nishimura et al. for laminar flow, using the geometry similar to that of Oxford membrane blood oxygenator [57, 73, 74, 75, 76, 77, 78].

Sparrow and Prata performed both experimental and numerical studies for laminar flow and heat transfer in a periodically converging-diverging tube and reported moderate enhancement due to the periodic area changes, but the pressure drops for the periodic tubes were substantially found greater than those for the straight tube [50]. Yalamanchili studied the centerline velocities and velocity profiles for fluid in a corrugated channel with the top and bottom plates sinusoidal with and without polymer additives, using laser Doppler velocimetery [6]. The presence of secondary flow in the channel was also observed as the aspect ratio of the plates increased.

Experiments were carried out in a horizontal rectangular water channel with bottom wall having sinusoidal waves and top wall flat by Buckles et al. [79]. This

experimental data is used as a reference for the validation of present numerical calculations for turbulent flow (Re=12,000), wavelength, $\lambda = 50.8\ mm$, aspect ratio, $2a/\lambda = 0.2$, and bulk velocity, $U_b = 51$ cm/s.

Saniei and Dini measured local heat transfer and pressure drop for the periodically converging-diverging bottom walled rectangular channel where the opposite top wall took one of the three following constructions: (1) plane; (2) converging-diverging, making in-phase arrangement with the bottom wall; (3) converging-diverging, making an out-of-phase arrangement with the bottom wall [80]. Measurements were performed for three different aspect ratios, and Reynolds number ranged from 22,000 to 52,000 in the turbulent region, to study heat transfer, pressure drop, and friction factor.

Chapter 3

Formulation of The Problem

3.1 Description of General Problem

Schematic view of the physical domain being considered is shown in Fig. 1.2. As seen, geometry is a periodically converging-diverging duct with sinusoidal walls in streamwise direction. The separation distance between the two walls varies sinusoidally with minimum height, H_{min}, maximum height, H_{max}, length of period, λ, and aspect ratio, $2a/\lambda$.

3.2 Periodic Fully Developed Flow Regime

The fluid flow in a periodically corrugated duct attains a periodic fully developed turbulent regime which differs from that of a straight duct. In the periodically corru-

gated duct, the periodic fully developed velocity field repeats itself at corresponding axial stations in successive cycles. In such a regime, the pressure varies cyclically at the corresponding locations and decrease linearly in the downstream direction. Similarly, a periodic thermally developed regime exists for commonly encountered boundary conditions such as uniform wall temperature and uniform wall heat flux, such a regime is characterized by a cycle average heat transfer coefficient [24].

3.3 Coordinate System

The calculation of the flow and heat transfer in converging-diverging duct in cartesian-coordinate system is quite laborious and inaccurate (because cartesian-coordinates are not coincident with the boundaries of solution domain). The main problem is the specification of boundary conditions because of the fact that the boundaries of the duct are not coincident with domain boundaries. Therefore for present calculations, orthogonal curvilinear coordinate system is used, as it coincides with the channel boundaries. To achieve this. the conservation equations of mass, momentum and energy were transformed from their cartesian coordinates to orthogonal curvilinear form through the appropriate tensor transformations [18]. The turbulence model equations of the kinetic energy of the turbulence and its dissipation rate were also transformed in the similar manner [19]. The whole set of equations is then integrated over the control volumes of an orthogonal curvilinear grid which is obtained

by Laplace grid generation technique.

3.4 Governing Equations

3.4.1 Mean Flow Equations

The governing equations are steady two-dimensional symmetric form of continuity and time-averaged incompressible Navier-Stokes equation. These equations for cartesian coordinates are written first in general tensor notation with Boussinesq approximation (i.e $\rho\overline{u'v'} = \rho\mu_t\frac{\partial\overline{u}}{\partial y}$) are given below [1];

Mass Conservation: Continuity equation

$$\frac{\partial}{\partial x_i}(\rho U_i) = 0 \tag{3.1}$$

Momentum Conservation: Navier-Stokes equation

$$\frac{\partial}{\partial x_i}(\rho U_i U_j) = -\frac{\partial p}{\partial x_j} + \frac{\partial}{\partial x_i}\left[(\mu_t + \mu)\frac{\partial U_j}{\partial x_i}\right] \tag{3.2}$$

where U_j is the time-averaged velocity component in the coordinate directions x_j, p is the local pressure, and ρ is the fluid density. In momentum equation, eddy viscosity hypothesis has been used, thus eddy viscosity, μ_t is specified according

to turbulence model. Using the same hypothesis, the time-averaged conservation equation of the thermal energy can be expressed by;

Thermal energy equation:

$$\frac{\partial}{\partial x_i}(\rho U_i \mathbf{H}) = \frac{\partial}{\partial x_i}\left[\left(\frac{\mu_t}{\sigma_t} + \frac{\mu}{\sigma}\right)\frac{\partial \mathbf{H}}{\partial x_i}\right] \tag{3.3}$$

The left hand side of this equation is the convective flux and the right hand is the diffusive flux.

3.4.2 Turbulence Modelling Equations

A two-dimensional, two-equation $k-\varepsilon$ model is used for the solution of the conservation equations, for the kinetic energy of turbulence and its rate of dissipation. The turbulence kinetic energy is given by [2];

$$\rho U_i \frac{\partial k}{\partial x_i} = \frac{\partial}{\partial x_i}\left[\left(\mu + \frac{\mu_t}{\sigma_k}\right)\frac{\partial k}{\partial x_i}\right] + G - \rho\varepsilon \tag{3.4}$$

The isotropic dissipation rate of the turbulent kinetic energy is given by [2];

$$\rho U_i \frac{\partial \varepsilon}{\partial x_i} = \frac{\partial}{\partial x_i}\left[\left(\mu + \frac{\mu_t}{\sigma_\varepsilon}\right)\frac{\partial \varepsilon}{\partial x_i}\right] + \frac{\varepsilon}{k}(C_{\varepsilon 1} f_1 G - C_{\varepsilon 2} f_2 \rho\varepsilon) + E' \tag{3.5}$$

where

μ_t = turbulent viscosity. $C_\mu f_\mu \rho \frac{k^2}{\varepsilon}$

Second last term in equation (3.5), $\rho\varepsilon$ is the destruction rate and G is the rate of generation of turbulent kinetic energy and is given by;

$$G = \mu_t \left[\left(\frac{\partial U_i}{\partial x_j} + \frac{\partial U_j}{\partial x_i} \right) \frac{\partial U_i}{\partial x_j} \right] \tag{3.6}$$

or

$$G = \mu_t \left[2 \left(\frac{\partial U}{\partial x} \right)^2 + 2 \left(\frac{\partial V}{\partial y} \right)^2 + \left(\frac{\partial V}{\partial x} + \frac{\partial U}{\partial y} \right)^2 \right] \tag{3.7}$$

At high Reynolds number where local isotropy prevails, the rate of dissipation, ε is equal to the kinematic viscosity times fluctuating vorticity. The isotropic dissipation rate ε is defined as:

$$\varepsilon = \nu \overline{\frac{\partial u_i'}{\partial x_j} \frac{\partial u_i'}{\partial x_j}} \tag{3.8}$$

An exact transport equation can be derived from the Navier-Stokes equation for fluctuating vorticity, and thus for the dissipation, ε. This contains complex correlation where behavior is little known and for which fairly drastic model assumptions must be introduced in order to make the equation tractable. The outcome of this modelling is the ε-equation (3.5). Together with the k-equation, ε-equation forms the so-called $k - \varepsilon$ turbulence model.

C_μ	$C_{\varepsilon 1}$	$C_{\varepsilon 2}$	σ_k	σ_ε	f_μ	f_1	f_2	E'
0.09	1.44	1.92	1.0	1.3	1.0	1.0	1.0	0.0

Table 3.1: Constants for $k-\varepsilon$ model [20]

Generally $k-\varepsilon$ model is only valid in regions where the flow is entirely turbulent. Close to the solid walls viscous effects becomes dominant and such a model does not lead to acceptable predictions. High Reynolds number $k-\varepsilon$ model is used for the present calculations, and its constants are given in Table 3.1.

3.4.3 Law of the Wall

The region close to solid walls can be divided into two sublayers

a) viscous sublayer : where purely viscous effects are dominant, i.e close to the solid wall.

b) turbulent sublayer : where inertial effects are dominant, i.e away from the solid wall.

It has been assumed that the first computational point P adjacent to the wall is in the turbulent sublayer, and in this sublayer the velocity has a logarithmic variations and conditions on the wall are related to lograthmic law of the wall [12].

3.5 Boundary Conditions

On each of the computational domain boundary conditions are required at: inlet, outlet, solid walls and symmetry axis. For each type and for each unknown, boundary conditions are to be specified.

3.5.1 Boundary Conditions for U_i and H

Solid walls

$$U_i = 0 \;\; \& \;\; T = \text{specified}$$

Inlet

$$U_i = \text{specified} \;\; \& \;\; T = \text{specified}$$

3.5.2 Boundary Conditions for $k - \varepsilon$

Turbulent Sublayer

According to the law of the wall, velocity U has logarithmic variation and given by [34].

$$|U_p| = \frac{u^*}{\kappa} ln(E y_p^+) \tag{3.9}$$

u^* is the friction velocity and y_p^+, is a dimensionless distance from point P to the wall;

$$u^* = \left(\frac{\tau_w}{\rho}\right)^{0.5} \tag{3.10}$$

$$y_p^+ = \frac{\rho y_p u^*}{\mu} \tag{3.11}$$

where

τ_w is the shear stress at the wall

κ is the Von Karman constant

E is a roughness parameter

y_p is the actual distance from point P to the wall

It is the value of the dimensionless distance y_p^+ that sets the limits between the different sublayers.

Supposing that the rate of k production is exactly equal to its destruction rate near the wall is given by [34];

$$\frac{\mu_t}{\rho}\left(\frac{\partial u}{\partial y}\right)^2 = \varepsilon \tag{3.12}$$

For solid walls with no slip at the boundary, it is not practical to carry out the computations down through the very thin, viscous sublayer. Assuming local

equilibrium by further supposing that the shear stress is constant in the sublayer ($\tau_p = \tau_w$), the law of the wall gives [12];

$$k_p = \frac{u^{*2}}{\sqrt{C_\mu}} \tag{3.13}$$

and

$$\varepsilon_p = \frac{u^{*3}}{\kappa y_p} \tag{3.14}$$

Equations (3.13) and (3.14) gave the values of k and ε at point P without solving the transport equations (3.3) and (3.4). In order to obtain u^*, equation (3.9) and (3.11) are combined to yield the non-linear equation;

$$|U_p| = \frac{u^*}{\kappa} ln\left(\frac{E\rho y_p u^*}{\mu}\right) \tag{3.15}$$

The velocity U_p is known from the solution of momentum equation (3.2). The values of k_p and ε_p are used to calculate the turbulent viscosity and serve as boundary conditions (*Dirichlet boundary conditions*) for the rest of the domain.

It is not necessary to calculate k and ε at the walls. The viscosity there is equal to the laminar viscosity.

3.5.3 Inlet

Values of k and ε are not known at the inlet but, if they are not given by experimental data, some reasonable assumptions can be made. The kinetic energy of turbulence

is estimated according to a certain percentage of the square of the average inlet velocity [12];

$$k = \beta \overline{u}^2 \tag{3.16}$$

where $\overline{u}$ is the average inlet velocity and β is constant.

The dissipation is calculated according to the equation [12];

$$\varepsilon = C_\mu \frac{k^{\frac{3}{2}}}{\alpha D_H} \tag{3.17}$$

where D_H is the inlet hydraulic diameter. The values $\alpha = 0.005$ and $\beta = 0.03$ are commonly used and may vary slightly [34].

3.5.4 Outlet

For any variable ϕ (excluding pressure) the condition is;

$$\frac{\partial \phi}{\partial x} = 0 \tag{3.18}$$

3.5.5 Symmetry axis

Setting here the derivative of the variables, equal to zero;

$$\frac{\partial \phi}{\partial y} = 0 \tag{3.19}$$

3.6 Orthogonal Curvilinear Coordinate System

The consideration and choice of coordinate system is discussed in this section. For the numerical solution of the differential flow equations about complex geometries, a suitable coordinate system has to be chosen. A numerical technique is applied on a mesh which is an ordered set of discrete points in that coordinate system. Therefore, solution necessary and computational expediency depends upon the mesh as well as the numerical technique. Accurate representation of boundary conditions and the resolution of the state variables in regions of rapid changes such as boundary layers and separated flow, require particular characteristics of the mesh. These characteristics are;

- the mesh should adapt to the physical boundary conditions can be applied without special considerations such as interpolation.
- the mesh should be concentrated in regions of rapid change to accurately capture the solution there

from the computational point of view, it is desirable that

- the mesh must be uniform, i.e. the boundaries should enclose simple rectangles
- the exterior boundaries of the rectangles correspond to physical boundaries.

The calculations of the flow and heat transfer in converging-diverging duct in cartesian coordinates are quite laborious and inaccurate. The main problem con-

cerning this is the specification of the boundary conditions because of the fact that the boundaries of the duct are not coincident with the domain boundaries. The best choice is, therefore, using an curvilinear grid of which the boundaries coincides with the domain boundaries [89].

Curvilinear coordinate can be orthogonal or non-orthogonal. The orthogonal has the advantage that the transformed partial differential equations are simpler than non-orthogonal ones. Thus results fewer computing operations, faster convergence, as well as better stability and accuracy of the solution. An additional disadvantage of orthogonal coordinates is the fact that there is no control on the locations of the grid points along the boundaries. During the grid generation process, these may shift along the boundaries, resulting in insufficient grid points near the sharp corners. In case of non-orthogonal coordinates it is much easier to have greater concentration of grid lines in the regions where good resolution is required. However, non-orthogonal coordinates introduce additional terms, which may reduce both convergence rate and stability and thereby increase the computing time. Also, the accuracy of the method is decreased because of the additional discretization approximations, necessary for the cross-derivative terms. Hence, it is often desirable to achieve orthogonality at least in the near-boundary regions where the gradients are the steepest and the cross-derivatives largest. Therefore, orthogonal curvilinear coordinate system is used for this problem.

3.7 Transformation of Equations

For computations orthogonal curvilinear coordinate system is used, that allows the coordinate lines to be arranged coincident with the flow boundaries. Equations in cartesian tensor notation are transformed in general orthogonal coordinates, which results in simple and compact expression of the equations which retains their physical significance. The advantage of the compact notation is that it leads to simple finite difference equations and consequently, to computational economy [19].

Orthogonal coordinate system in two dimensional is shown in Fig.3.1, where the orthogonal coordinates, ξ are shown in relative to cartesian coordinates, x_i. Distances in the general orthogonal coordinate system are related to the Cartesian system through the metric tensor g_{ij} by [89];

$$g_{ij} = \sum_l \frac{\partial x_l}{\partial \xi_i} \frac{\partial x_l}{\partial \xi_j} \tag{3.20}$$

where the scale factor h, is given by;

$$h_i = (g_{ii})^{1/2} \text{ (no summation on } i) \tag{3.21}$$

The physical components of displacement $h_i d\xi_i$, which are defined by equation (3.21), represent displacements along coordinate lines measured relative to the coordinate system x. Similarly, the physical components of a contravarient vector are

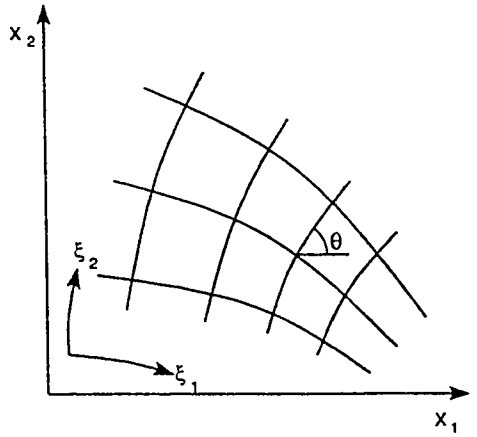

Figure 3.1: Orthogonal coordinate lines in cartesian coordinates. x

given by;

$$A(i) \equiv h_i A_i \tag{3.22}$$

and represent the components of the vector in the direction of the coordinate lines measured relative to the Cartesian system.

The steady-state differential equations in orthogonal curvilinear coordinates are given below;

Equation of continuity:

$$\nabla_i(U_i) = 0 \tag{3.23}$$

Navier-Stokes equation:

$$\nabla_i[\rho U_i U_j + \tau_{ij}^*] = -\frac{\partial p^*}{\partial \xi_j} + H_i(j)[\rho U_i U_i + \tau_{ii}^*] - H_j(i)[\rho U_i U_j + \tau_{ij}^*] \tag{3.24}$$

Thermal energy equation:

$$\nabla_i \left[\rho U_i H - \left(\frac{\mu_t}{\sigma_\phi} + \mu\right) \frac{\partial \phi}{\partial x_i}\right] = S_\phi \tag{3.25}$$

where components of the turbulent stress have been added to the pressure, i.e,

$$p^* = p + \frac{2}{3}\rho k + \frac{2}{3}\left(\frac{\mu_t}{\mu_o} + \mu\right) \nabla_i(U_i) \tag{3.26}$$

and τ^* contains the anisotropic stresses is given by;

$$\tau_{ij}^* = -\left(\frac{\mu_t}{\mu_\phi} + \mu\right)\left[\frac{\partial U_i}{\partial \xi_j} + \frac{\partial U_j}{\partial \xi_i} - U_i H_i(j) - U_j H_j(i) + 2U_l H_i(l)\delta_{ij}\right] \qquad (3.27)$$

The production of turbulent kinetic energy is given by;

$$G = -\tau_{ij}^*\left[\frac{\partial U_j}{\partial \xi_j} - U_j H_j(i) + U_l H_i(l)\delta_{ij}\right] - \frac{2}{3}\left[\rho k + \left(\frac{\mu_t}{\sigma_\phi} + \mu\right)\nabla_i U_i\right]\nabla_l U_l \qquad (3.28)$$

The physical interpretation of the scalar transport equation is straight forward and is not unexpected, the inflow of ϕ due to convective and gradient diffusion is balanced by the source. The same form is adopted by the continuity equation but the momentum equation has gained source terms reflects the fact that momentum is conserved in a straight line. Thus, for example, the term;

$$S_j = H_i(j)\rho U_i U_i - H_j(i)\rho U_i U_j$$

represents a transfer of momentum from one coordinate direction to another and, since $S_j Uj$ is zero, the transfer is conservative. That is, S_j affects the direction of the velocity vector relative to the orthogonal coordinate system but not its length, since the source due to S_j in the equation for $U_i U_j$ is zero. The additional terms in relations for the stress tensor and the production of kinetic energy arise from the transformation of the velocity gradient and, as can be seen, G can be expressed as the sum of an identically non-negative terms due to the rate-of-strain and a term due to the divergence of velocity.

3.8 General form of Differential Equations

The general compact form of elliptic differential equation governing the two-dimensional recirculating flow is given by [28];

$$\frac{\partial}{\partial x}(\rho U\phi) + \frac{\partial}{\partial y}(\rho V\phi) = S_\phi + \frac{\partial}{\partial x}\left(\Gamma_\phi \frac{\partial \phi}{\partial x}\right) + \frac{\partial}{\partial y}\left(\Gamma_\phi \frac{\partial \phi}{\partial y}\right) \qquad (3.29)$$

The description of turbulent flows in this way presumes that the time mean values of the dependent variables of the turbulent flow, i.e, ϕ, can be represented by this form of equation. Table 3.2 lists these variables alongwith Γ_ϕ and S_ϕ.

$$G = \mu_e \left\{ 2\left[\left(\frac{\partial U}{\partial x}\right)^2 + \left(\frac{\partial V}{\partial y}\right)^2\right] + \left(\frac{\partial W}{\partial x}\right)^2 + \left(\frac{\partial W}{\partial y}\right)^2 + \left(\frac{\partial U}{\partial y} + \frac{\partial V}{\partial x}\right)^2 \right\} \qquad (3.30)$$

The general differential equation in the orthogonal curvilinear coordinate system can be written as [20];

$$\nabla_{\xi_1}\left(\rho U\phi - \Gamma_{\phi_1}\frac{\partial \phi}{\partial \xi_1}\right) + \nabla_{\xi_2}\left(\rho V\phi - \Gamma_{\phi_2}\frac{\partial \phi}{\partial \xi_2}\right) = S_\phi \qquad (3.31)$$

and the variables in general form are given in Table 3.3

$$G = \frac{1}{2\mu_e}[\tau^2_{\xi_1\xi_1} + \tau^2_{\xi_2\xi_2} + \tau^2_{\xi_3\xi_3} + 2(\tau_{\xi_1\xi_2} + \tau_{\xi_2\xi_3} + \tau_{\xi_3\xi_1})^2] \qquad (3.32)$$

The difference between this equation and its cartesian counterpart lie solely in the divergence operator and the source terms and consequently, it is possible to

Conservation of	o	Γ_o	S_o
Mass	1	0	0
Axial Momentum	U	μ_e	$-\frac{\partial p}{\partial x}+\frac{\partial}{\partial x}(\mu_e\frac{\partial U}{\partial x})+\frac{\partial}{\partial y}(\mu_e\frac{\partial V}{\partial x})$
Radial Momentum	V	μ_e	$-\frac{\partial p}{\partial y}+\frac{\partial}{\partial x}(\mu_e\frac{\partial U}{\partial x})+\frac{\partial}{\partial y}(r\mu_e\frac{\partial V}{\partial y})$ $-2\mu_e\frac{V}{y^2}+\rho\frac{W^2}{y}$
Tangt. Momentum	W	μ_e	$-(\frac{\mu_e}{y^2}+\rho\frac{V}{y}+\frac{\partial\mu_e}{\partial y})W$
Turbulent K.E.	k	μ_e/σ_k	$G-\rho\varepsilon$
Dissipation rate	ε	μ_e/σ_ε	$\frac{\varepsilon}{k}(C_1G-C_2\rho\varepsilon)$
Enthalpy	**H**	μ_e/σ_k	0

Table 3.2: Conservation equations corresponding to equation (3.29) [28]

ϕ	Γ_{ϕ_1}	Γ_{ϕ_2}	S_ϕ
1	0	0	0
U	μ_e	μ_e	$-\frac{\partial p}{\partial \xi_1} + \nabla_{\xi_1}\{\mu_e[\frac{\partial U}{\partial \xi_1} + 2VH_1(2)]\} + \nabla_{\xi_2}\{\mu_e[\frac{\partial V}{\partial \xi_1}$ $-H_1(2)U - H_2(1)V]\} + H_2(1)\{\rho V^2 - \mu_e[2\frac{\partial V}{\partial \xi_2}$ $+2UH_2(1)]\} + H_3(1)\{\rho W^2 - \mu_e[2UH_3(1) + 2VH_3(2)]\}$ $-H_1(2)\{\rho UV - \mu_e[\frac{\partial U}{\partial \xi_2} + \frac{\partial V}{\partial \xi_1} - H_1(2)U - H_2(1)V]\}$
V	μ_e	μ_e	$-\frac{\partial p}{\partial \xi_2} + \nabla_{\xi_2}\{\mu_e[\frac{\partial V}{\partial \xi_2} + 2UH_2(1)]\} + \nabla_{\xi_1}\{\mu_e[\frac{\partial U}{\partial \xi_2}$ $-H_2(1)V - H_1(2)U]\} + H_1(2)\{\rho U^2 - \mu_e[2\frac{\partial U}{\partial \xi_1}$ $+2VH_1(2)]\} + H_3(2)\{\rho W^2 - \mu_e[2VH_3(2) + 2UH_3(1)]\}$ $-H_2(1)\{\rho UV - \mu_e[\frac{\partial V}{\partial \xi_1} + \frac{\partial U}{\partial \xi_2} - H_2(1)V - H_1(2)U]\}$
W	μ_e	μ_e	$-\nabla_{\xi_1}[\mu_e H_3(1)W] + \nabla_{\xi_2}[\mu_e H_3(2)W] - H_3(1)[\rho UW$ $-\mu_e\frac{\partial W}{\partial \xi_1} + \mu_e H_3(1)W] - H_3(2)[\rho VW - \mu_e\frac{\partial W}{\partial \xi_2}$ $+\mu_e H_3(2)W]$
k	μ_e/σ_k	μ_e/σ_k	$G - \rho\varepsilon$
ε	μ_e/σ_ε	μ_e/σ_ε	$\frac{\varepsilon}{k}(C_1G - C_2\rho\varepsilon)$
$\mathbf{H}$	μ_e/σ_h	μ_e/σ_h	0

Table 3.3: Conservation equations corresponding to equation (3.31) [20]

obtain a finite-difference procedure for orthogonal coordinates by modifying it for cartesian coordinates.

Chapter 4

Finite Difference Formulation

4.1 Numerical Solution

A numerical solution of a differential equation consists of a set of a numbers from which the distribution of the dependent variables ϕ, can be constructed. Derivation of finite difference equations is obtained by discretizing the partial differential equations. The entire flow domain is divided into the control-volumes with grids at their geometric centers and all the variables defined at those grid points. With sufficiently fine grids, the complete distributions of the relevant variables can be expressed in terms of their values at each grid point.

4.1.1 Domain Discretization

In order to solve the differential equations an orthogonal grid has been generated, the relations between the distances in orthogonal coordinate system and cartesian system is discussed earlier in chapter 3. The orthogonal grid transformed the irregular shaped orthogonal rhombus of the finite volume grid in physical space (X_i) transforming it into uniform rectangular computational space (ξ_i) in which the final transformed governing equations are solved. An orthogonal curvilinear mesh is obtained from an inverse solution of the Laplace equations. A number of grid lines with even spacing is produced by the method of interpolation to provide the number of nodes appropriate to the flow problem and the required economy and numerical accuracy. Selectively refined grid is used to retain numerical accuracy in the regions of high gradients, and close to the boundaries.

The computational domain in the orthogonal curvilinear coordinate is discretized by placing grid points at the geometric centers of the control-volumes drawn in an arbitrary non-uniform manner. In this practice a control-volume face is not midway between the adjacent grid points. This yields a less accurate finite-difference representation of the derivatives.

4.1.2 Control-Volume Formulation

The basic idea of the control-volume formulation is that the solution domain is divided into a number of non-overlapping control-volumes such that there is only one control-volume surrounding each grid point. The differential equation is integrated over each control-volume. Thus, discretization equation represents the same conservation principle over a finite region as the differential equation does over an infinitesimal region. This expresses the variation of ϕ between the grid points to evaluate the required integrals. The result is the discretization equation containing the values of ϕ for a group of grid points.

Attractive feature of control-volume formulation is that the resulting solution would imply that the integral conservation of quantities such as mass, momentum and energy is exactly satisfied over any group of control-volumes and, over whole calculation domain.

Control-volume formulation is a special version of method of weighted residuals, in which the weighting function is chosen to be unity over a control-volume and zero everywhere else [82]. The main reasons for choosing the control-volume formulation are the simplicity and easy physical interpretation.

4.2 Finite Difference Equations

4.2.1 Interior Control-Volumes

For the required solution the flow domain is overlaid with an orthogonal curvilinear grid whose intersection points or nodes denote the location at which all variables (with the exception of velocities) are calculated. The velocities are computed at locations midway between the pressure which drive them. Thus the normal velocity components are directly available at the control-volume faces, where they are needed for the calculation of mass flow rates. The nodes of a typical grid cluster are labelled as P, N, S, E and W which lies on lines of constant ξ_1 and ξ_2.

The finite difference counterparts of the general PDE (see chapter 3, equation (3.31)) is derived by supposing that each variable is enclosed in its own control-volume. The PDE is integrated over the control-volume, with the aid of assumptions about the relations between the nodal values at P and the rates of creation/destruction of this entity within the cells and its transport by convection and diffusion across the cell boundaries.

The finite-difference equations are obtained by integrating the equations over the (two-dimensional) volume indicated on the finite-difference grid is shown in Fig. 4.1. The values of the variable ϕ in question is assumed to be known at the node P, and its four nearest neighbors N, S, E and W. The intersections of the main grid lines and the cell faces are designated n, s, e and w. The integration yields:

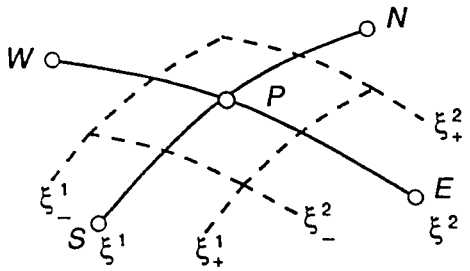

Figure 4.1: Finite-difference cell

$$\int_s^n \int_w^e \nabla_{\xi_1} \left(\rho U \phi - \Gamma_{\phi_1} \frac{\partial \phi}{\partial \xi_1} \right) d\xi_1 d\xi_2 + \int_s^n \int_w^e \nabla_{\xi_2} \left(\rho V \phi - \Gamma_{\phi_2} \frac{\partial \phi}{\partial \xi_2} \right) d\xi_1 d\xi_2 = \int_s^n \int_w^e S_\phi d\xi_1 d\xi_2 \tag{4.1}$$

or

$$\left[\left(\rho U \phi - \Gamma_{\phi_1} \frac{\partial \phi}{\partial \xi_1} \right) \Delta \xi_2 \right]_w^e + \left[\left(\rho V \phi - \Gamma_{\phi_2} \frac{\partial \phi}{\partial \xi_2} \right) \Delta \xi_1 \right]_s^n = S_\phi \Delta \xi_1 \Delta \xi_2 \tag{4.2}$$

if we now denote the integrated total flux across a face by J i.e

$$J = (\rho U \phi - \Gamma_\phi \frac{\partial \phi}{\partial \xi}) \Delta \xi \tag{4.3}$$

which can be further divided into the convective flux C, and the diffusion flux D, i.e

$$C = \rho U \phi \Delta \xi \tag{4.4}$$

$$D = \Gamma_\phi(\frac{\partial \phi}{\partial \xi})\Delta\xi \tag{4.5}$$

and linearize the source term in the form

$$S_\phi = S_o + S_p o_p \tag{4.6}$$

then equation (4.2) becomes:

$$J_e - J_w + J_n - J_s = (S_o + S_p o_p)\Delta\xi_1\Delta\xi_2 \tag{4.7}$$

The task remaining now is to discretize the convective and diffusive flux terms. The diffusion flux is handled conveniently by the central difference and can be represented by expression of the form, for example:

$$D_e = \Gamma_\phi \frac{\partial \phi}{\partial \xi_1}\Delta\xi_2 = \Gamma_{\phi_e}\frac{(o_e - o_p)}{\Delta\xi_{PE}}\Delta\xi_{2e} \tag{4.8}$$

where the grid Peclet number, ratio of mean-flow convection to molecular diffusion is defined as [13]

$$Pe_e \equiv \frac{\rho U_e \Delta\xi_{PE}}{\Gamma_{\phi_e}} \tag{4.9}$$

Discretizing the convective flux depending on the grid Peclet number by the well known Hybrid Scheme [13].

$$\rho U_e \frac{(\phi_e + \phi_p)}{2} \Delta\xi_{2e} \quad \text{if} \quad |\, Pe_e \,| \leq 2$$

$$C_e = \rho U_e \phi_E \Delta\xi_{2e} \quad \text{if} \quad Pe_e > 2$$

$$\rho U_p \phi_P \Delta\xi_{2e} \quad \text{if} \quad Pe_e < -2$$

substituting the above conditions in equation (4.9) and (4.3), yields an expression for J_E for a given Peclet number. Exactly similar expressions can be obtained for J_w,J_s and J_n. These when substituted in equation (4.7) leads to the following finite difference equation expressing ϕ_p, the value of ϕ at that location, in terms of the values at the nearest neighboring nodes is;

$$(A_p - S_p)\phi_p = A_n\phi_n + A_s\phi_s + A_e\phi_e + A_w\phi_w + S_o \tag{4.10}$$

where $A_p = \Sigma_n A_n$; and S_o, and S_p are deduced from the S_ϕ of Table 3.3. Equations of this kind are written for each of the variable: U, V, k, ε, and h, at every cell.

4.2.2 Near-Boundary Control-Volumes.

The control-volumes adjacent to the boundary are dealt separately, by the *Law of the Wall* and has been discussed previously, so that the uniform approach can be made in matching the boundary conditions to the interior for all ϕ variables, and all flow conditions.

4.3 The Calculation Procedure

If the pressure field which appears as a major part of the source term is known, then equation (4.10), written for each grid node, yields a closed set of algebraic equations, but there is no guarantee that the resultant velocity field would satisfy the continuity relation. The two problems of determining the pressure and satisfying continuity are overcome by adjusting the pressure field.

4.3.1 Solution Algorithm

As discussed before a staggered grid arrangement is used in which the velocities are stored at a location midway between the grid points, i.e on the control-volume faces. All other variables including pressure are calculated at the grid points. This arrangement gives a convenient way of handling the pressure linkage through the continuity equation and is known as the SIMPLE (*Semi-Implicit Method for Pressure-Linked Equations*) algorithm developed by Patankar [13], which has been applied successfully by Asako et al. [15, 38], and others. Slightly modified versions are used by Grag et al. [44] and Patel et al. [7], for the flow in corrugated channels. This method is an iterative process to steady-state convergence. The mathematical development of this procedure focuses on providing a pressure link between continuity and momentum equations. This is accomplished by transforming the continuity equation into a Poisson equation for pressure. The Poisson equation implements a

pressure correction for velocity field. The staggered grid arrangement is employed to compensate for non-physical oscillations manifestation in the pressure distribution. These oscillations are due to a physical decoupling of the local pressure distribution from the local velocity field, as the pressure gradient in the momentum equations is discretized by central differences. The steady-state convergence is achieved by successively predicting and correcting the velocity components and the pressure variable. An initial guess for the pressure variable at each grid point is required.

Equation (4.10) with the pressure gradient separated from the source term can be rewritten for the U-velocity at the node for example;

$$(A_e - S_c^*)U_e = \Sigma A_{nb}\phi_{nb} + S_o^* + (p_P - p_E)\Delta\xi_{2e} \tag{4.11}$$

if p^* represents a guessed pressure at node P, and U_e^* and V_n^* represents the corresponding velocities calculated by equations similar to equation (4.11), then actual pressure is given by:

$$p = p^* + p' \tag{4.12}$$

Now a velocity-correction formula for velocity at node e for example can be written as;

$$U_e = U_e^* + \frac{\Delta\xi_{2e}}{A_e}(p'_P - p'_E) \tag{4.13}$$

in this expression certain assumptions have been made therefore U_e does not repre-

sents the exact value.

An equation very similar to equation (4.10) can be now written for p' by the discretization for the continuity equation and using equation (4.13).

$$(A_p - S_p)p'_p = A_n p'_n + A_s p'_s + A_e p'_e + A_w p'_w + S_o \tag{4.14}$$

Chapter 5

Results and Discussion

This chapter presents the numerical results of the flow field and forced convection heat transfer in the sinusoidal periodically converging-diverging channel with different amplitudes and Reynolds number.

5.1 Validation

For the validation of the present computational method, experimental work by Buckles et al. is chosen as the basis of comparison [79]. This would ensure that the turbulence model and the numerical method used are quite successful in capturing, most of the important physical features of such flows.

The geometry of Buckles et al. is shown in the Fig. 5.1, with flat wall at the top and bottom wall varying sinusoidally, making it periodically converging-diverging

channel, with minimum height, H_{min}=47.4mm and width, W=610mm. The aspect ratio, $2a/\lambda$=0.2 with an amplitude, a=5.08mm, and length of the module, λ=50.8mm. There are total of seven modules considered in the channel.

The results presented in this study are obtained by using nonuniform 30×24 grid. To assess the numerical accuracy, calculations are performed using two other coarser 26×20 and 20×15 grids. Velocity profiles at x/λ=0.5, where channel height is maximum, are plotted for these three computational grids, are shown in Fig. 5.2. Only minor difference is observed for these three different grid arrangements. Therefore, to ensure grid size convergence, all subsequent calculations are performed using 30×24 grid for each module.

Converging the solution, requires 250 iterations, taking approximately 20 minutes (execution time) to complete. All the calculations are performed at the sixth module, to allow the flow to become fully developed.

Also supplementary runs were performed with grid size of 26×20 and 20×16, to investigate the effect of grid size on the accuracy and convergence rate. Hence grid independence is checked, as the grid size decreases the convergence rate increases, that can be seen in Fig. 5.3.

5.1.1 Velocity Profiles

Fig. 5.4 shows the normalized axial velocity profiles at different intervals over a module. The solid lines represents the numerically obtained results and the circles

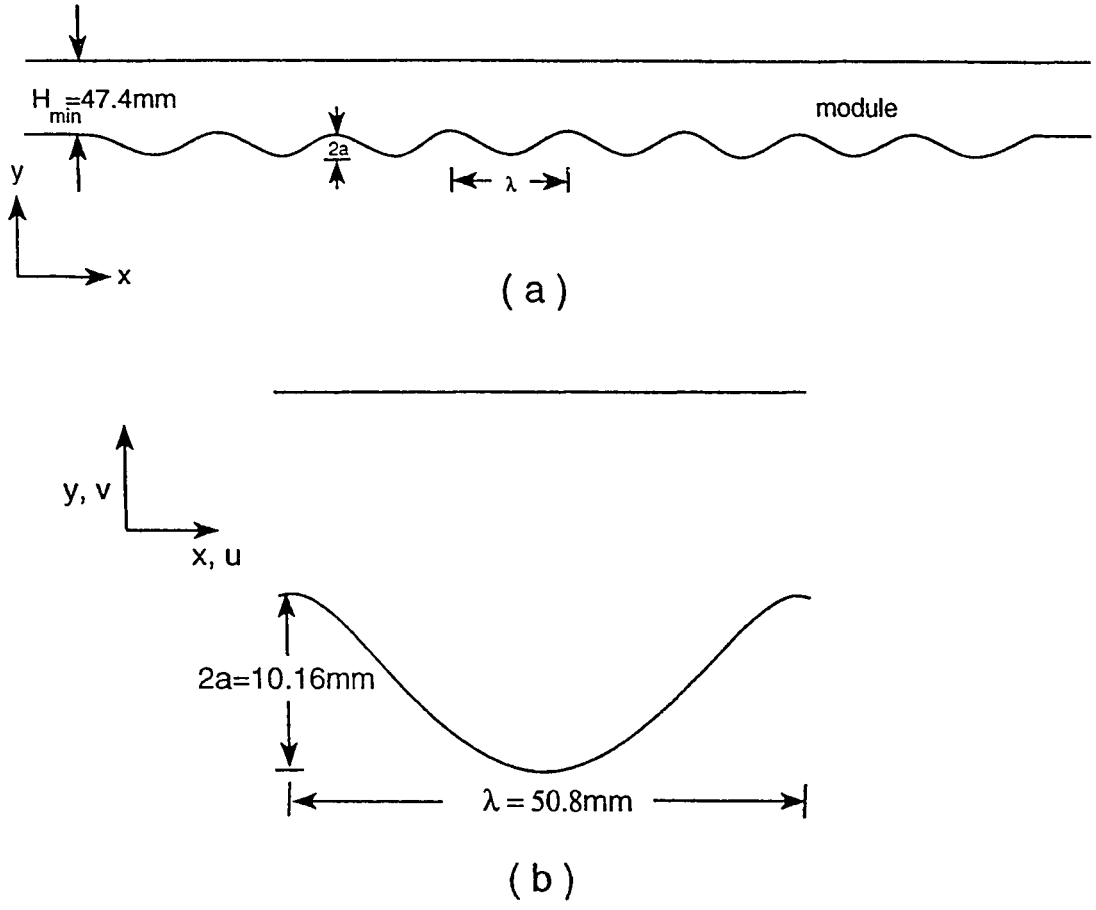

Figure 5.1: Periodically converging-diverging channel $2a/\lambda$=0.2

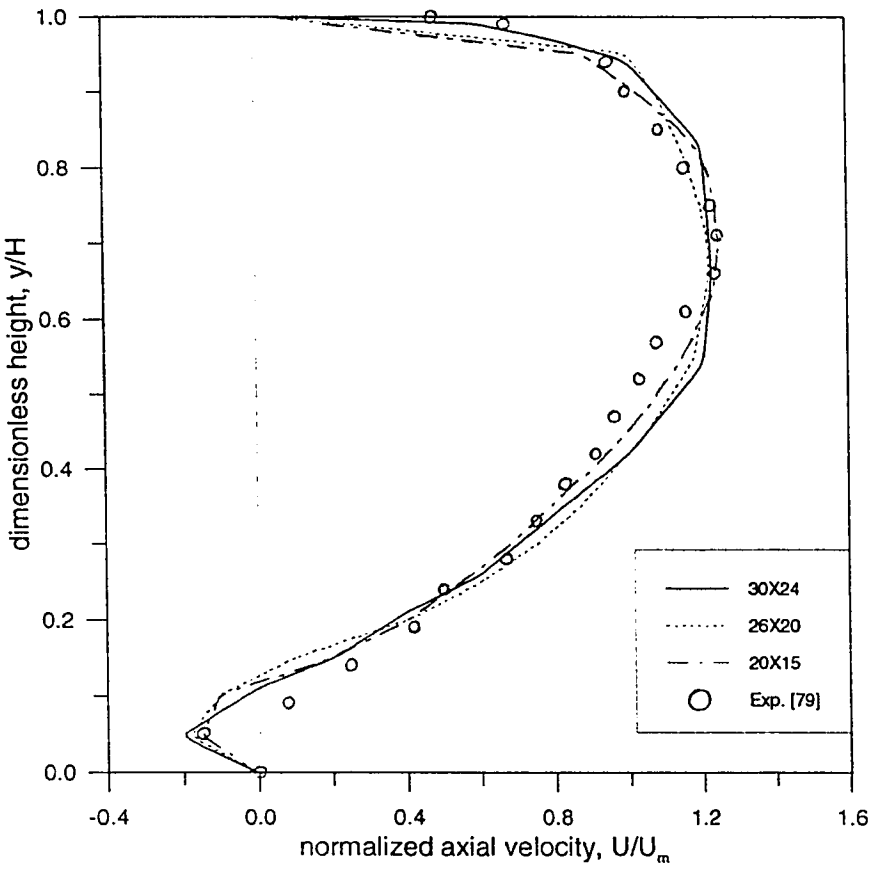

Figure 5.2: Velocity profiles for three different grid arrangements for $2a/\lambda = 0.2$ and Re=12,000

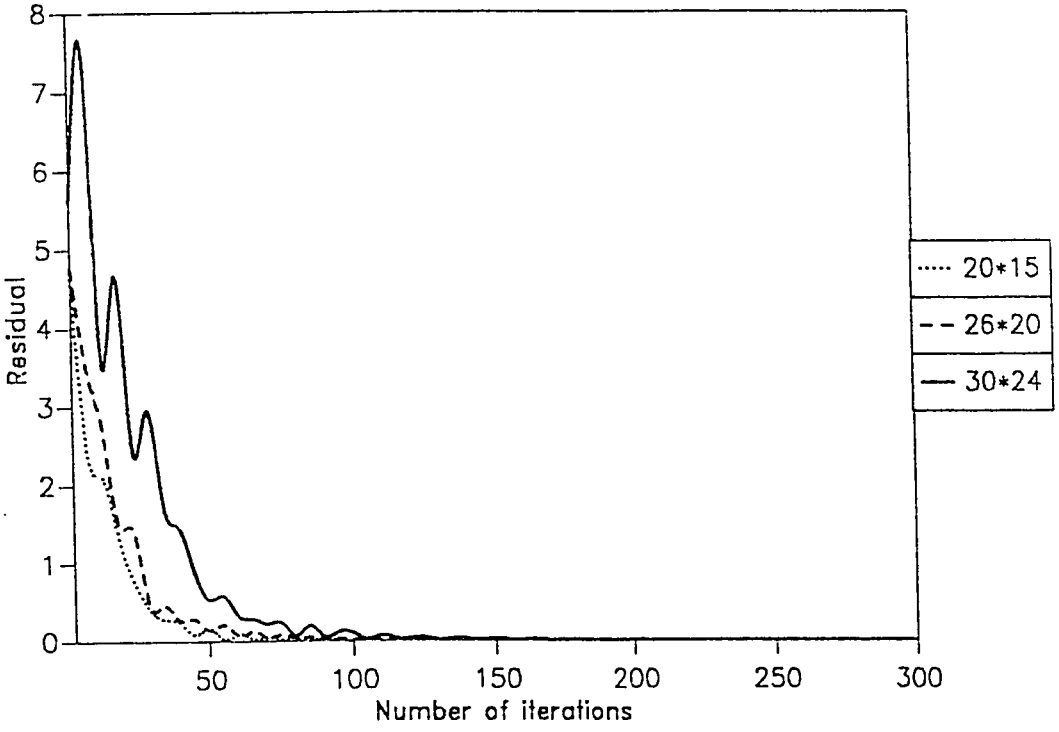

Figure 5.3: Dependence of convergence rate upon grid size for $2a/\lambda$=0.27

are the experimental data by Buckles et al. [79].

In Fig. 5.4, the position of x/λ=0.0 and 1 corresponds to the inlet and outlet of the 6th converging-diverging module, where the channel height is minimum, and x/λ=0.5 corresponds to the midpoint of the 6th cycle, where the channels height is maximum. It can be seen that as the channel diverges the flow decelerates, causing separation. This effect is obvious between x/λ=0.4 to 0.6 and the flow reattaches between x/λ=0.6 to 0.7. The calculated velocities are found larger than the measured ones, this is because the channel used in these experiments, the test section begins at the distance of 70 hydraulic diameters, it is possible that the end-wall effects are responsible for these higher core velocities. The agreement between the calculated and experimental results is good.

5.2 Sinusoidally Converging-Diverging Channel Flow

The numerical calculations performed are based on the geometry similar to that of Saniei and Dini [80], with channel height, H_{max}=10.16 cm and width, W=50.8 cm. The surface geometry included seven continuous corrugations varying sinusoidally, both on the top and bottom wall of the channel. Peak-to-peak distance between two corrugations is, λ=6.667 cm, and called as module (shown in Fig. 5.5). These corrugations covered about 47 cm of the length of the duct and spanned over the

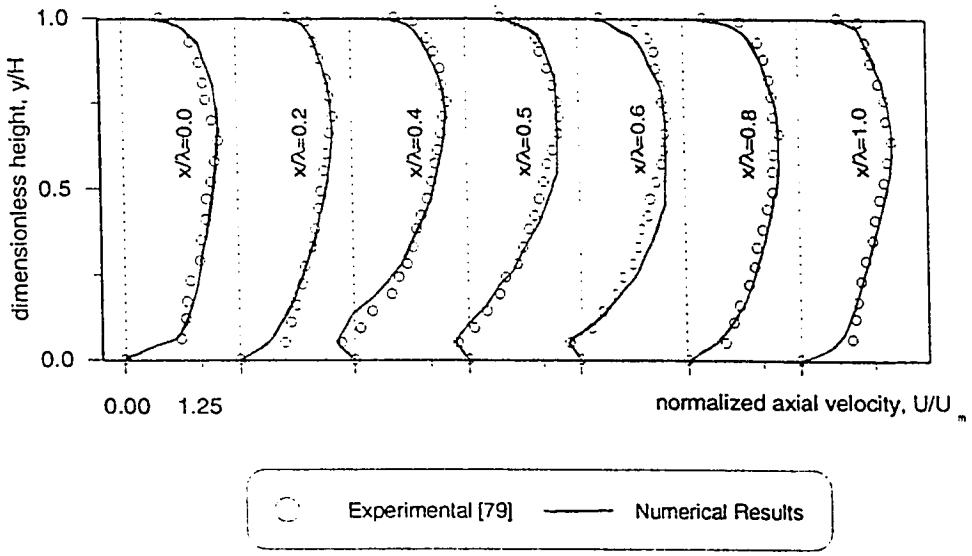

Figure 5.4: Velocity profiles at different locations, $2a/\lambda$=0.2, Re=12,000

entire width of the channel. For numerical study, two different aspect ratios (height-to-wavelength ratios) $2a/\lambda = 0.27$ and 0.34 are used. These studies are made for the Reynolds number based on hydraulic diameter of the channel varying from 40,000 to 100,000.

The experiments performed by Saniei and Dini [80] for symmetric converging-diverging periodic channel, provide the experimental data for the comparison of heat transfer with the present numerical work.

5.2.1 Computational Domain

The computational domain with uniform orthogonal curvilinear grids of points (32×32), is shown in Fig. 5.6, with an order of interpolation, $N = 250$. As the channel is symmetric, only half of the flow domain is solved, where the other half is similar. The measurements are taken after 5λ, so that the flow become periodically fully developed.

For the computational accuracy at the points of large variations in cross-sectional areas, i.e near the boundary, non-uniform grids of size 30×24 is chosen, with greater concentration near the wall as shown in Fig. 5.7. Thus for one module there are 720 nodes. Six hundred iterations were used, taking approximately 60 minutes on IBM 3090, to converge with residual of $\leq 10^{-4}$ for U-velocity.

The under-relaxation factors (URF) used for the different governing equations are given in table 5.1

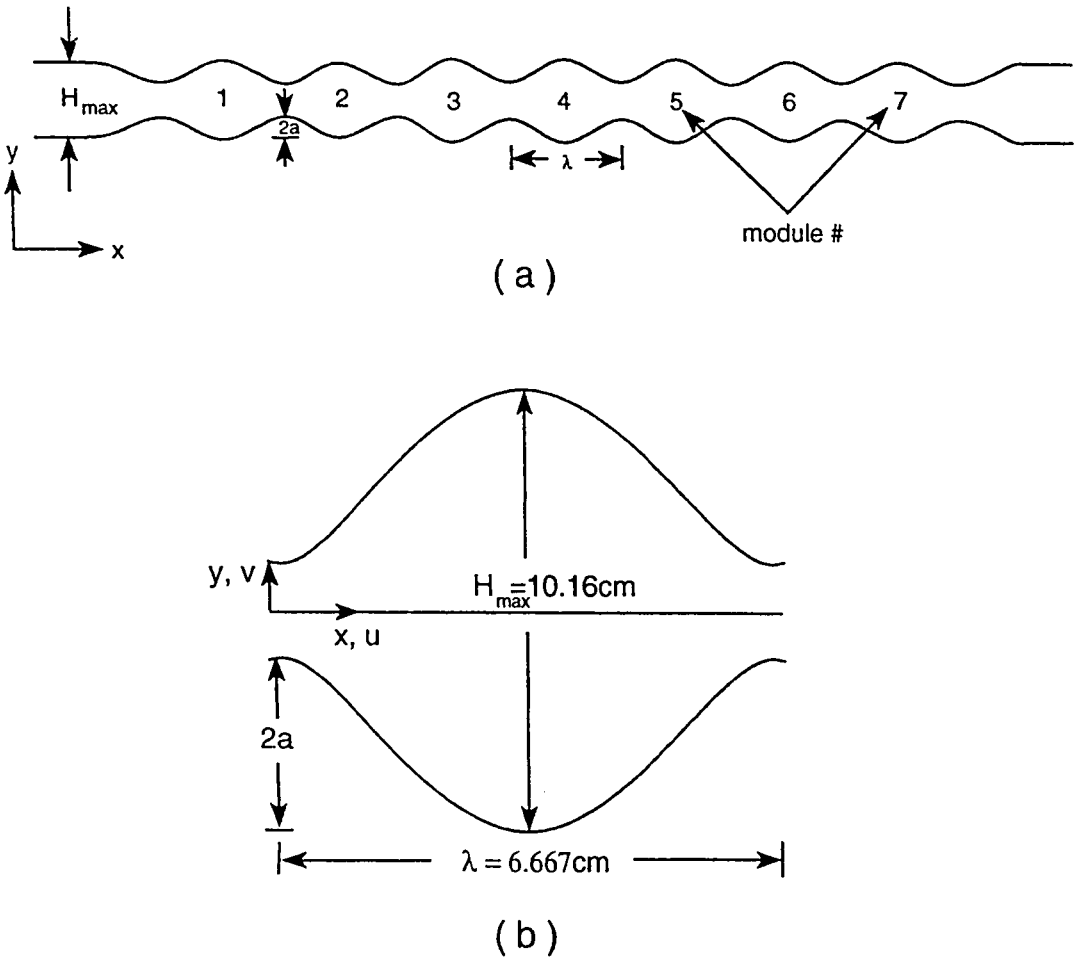

Figure 5.5: Sinusoidally converging-diverging channel

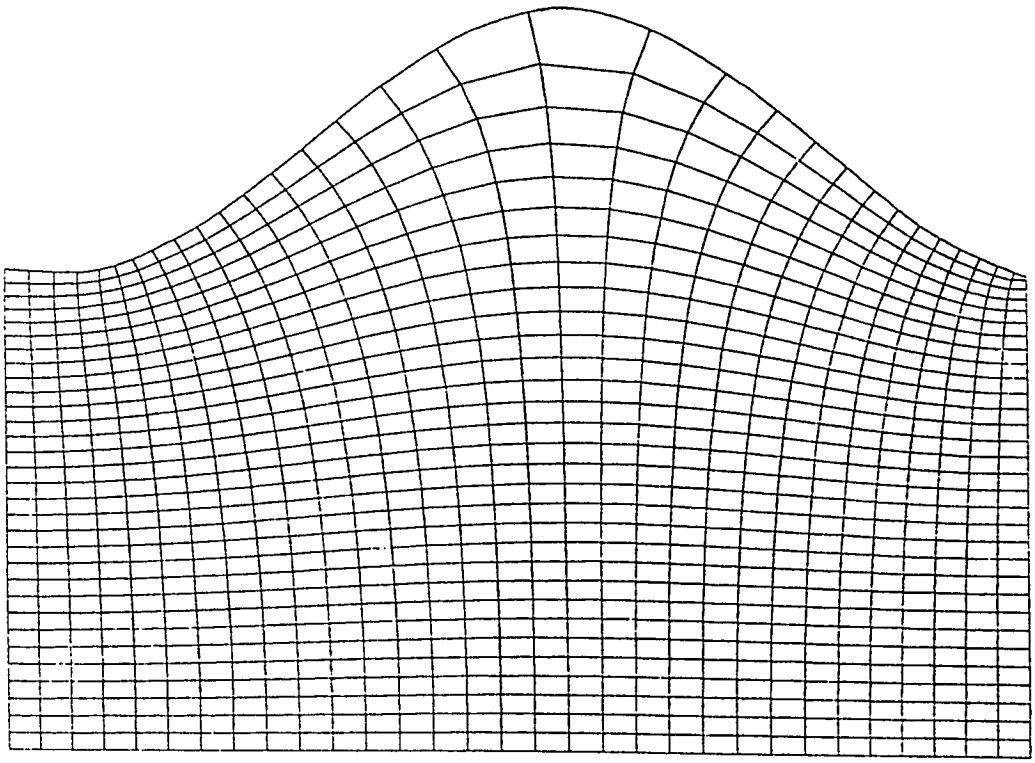

Figure 5.6: Solution domain with uniform orthogonal grid (32×32) for $2a/\lambda = 0.27$

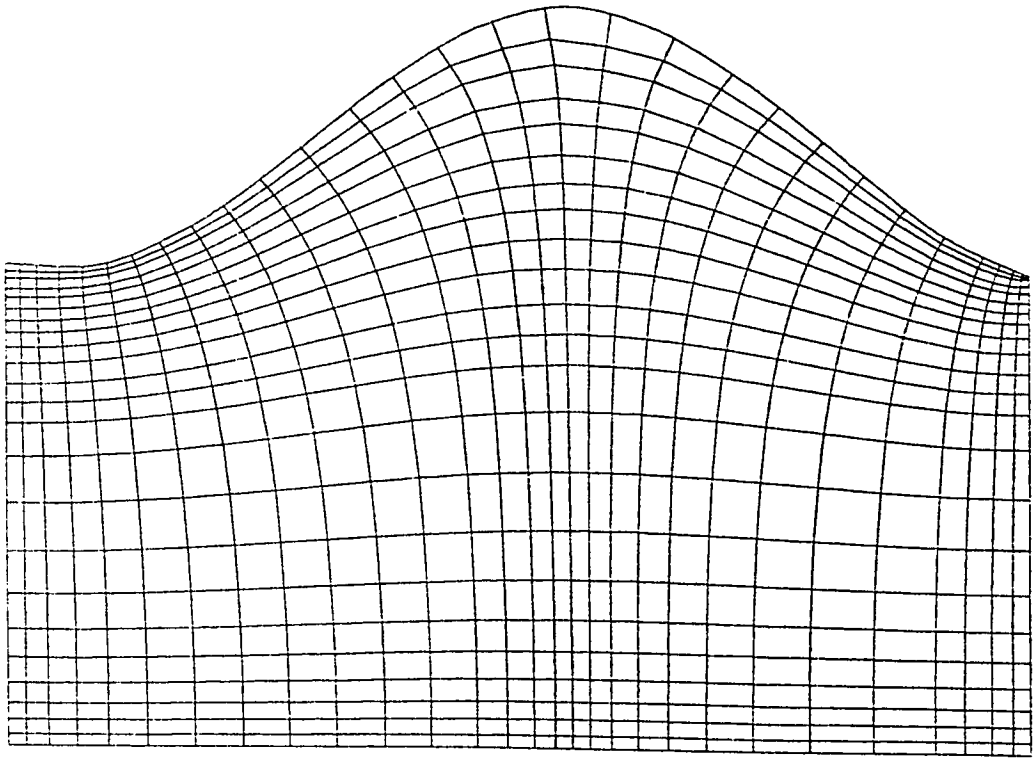

Figure 5.7: Solution domain with non-uniform grid (30 × 24) for $2a/\lambda = 0.27$

Variable	U	V	P	W	k	ε	H
URF	0.5	0.5	1.0	0.6	0.6	0.6	0.5

Table 5.1: Under-relaxation factors (URF) for different variables

5.2.2 Velocity Profiles

Figure 5.8 shows velocity distribution, normalized by the average velocity (U/U_{avg}) for amplitude of $2a/\lambda = 0.27$ and 0.34 respectively for two different Reynolds number, at various locations ($x/\lambda = 0$ to 1) of the sixth module.

It is observed that the velocity profiles remain unchanged upto $x/\lambda = 0.2$, in the decelerating section, however, the velocity profiles are affected by the change of the aspect ratio, causing larger changes in velocity profile in the streamwise directions. The deceleration is clearly seen at $x/\lambda = 0.4$ to 0.6 for both $2a/\lambda = 0.27$ and 0.34. For $2a/\lambda = 0.34$, the change in velocity profiles during a cycle is larger than that for $2a/\lambda = 0.27$. At the maximum cross-sectional area U-component of velocity is negative, near the wall. This is due to the effect of flow inertia on the velocity profiles. Note that in the diverging part of the channel the profiles are flattened at the centerline.

From these figures it is evident that the separation increases with the increase in Reynolds number and wall amplitude. This is because the back flow becomes stronger as well as more extensive. There exist a good agreement between this computed and experimental results by Patel et al. [7].

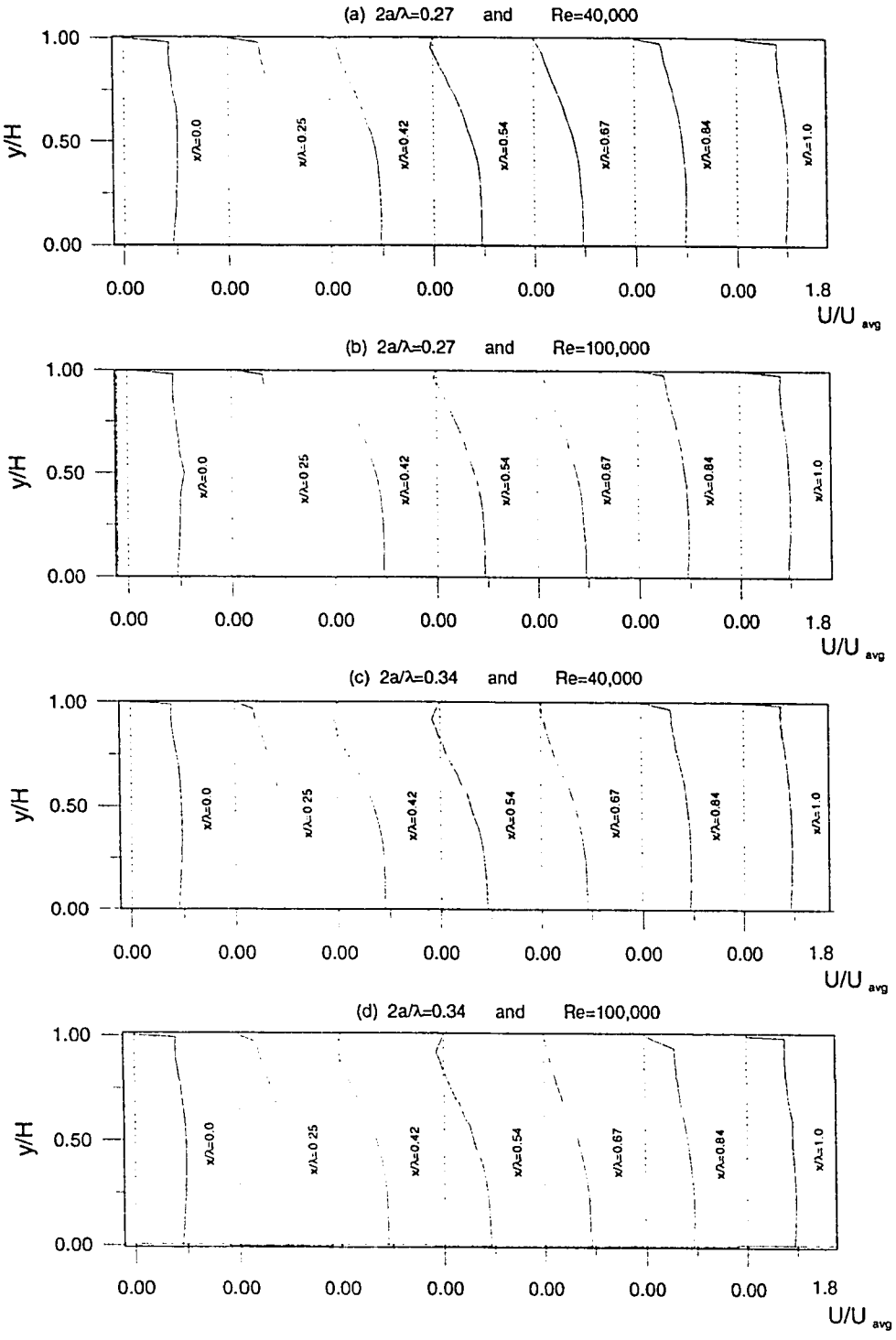

Figure 5.8: Normalized axial velocity profiles at different Reynolds number and aspect ratios at various locations in a module

In Fig. 5.9 the velocity profiles at sixth module for $2a/\lambda$=0.27 and $Re = 40,000$ is shown. The effect of increase in flow area and retardation of fluid layers relative to each other can be seen as a decrease in magnitude of axial velocity. However, similarity can be seen in velocity profiles at same cross-sectional area (upstream and downstream from the point of maximum height), with slight decrease in magnitude downstream. This is either because of the disturbances due to recirculation, or because of the model used. Near the wall (y/H=1), zones of separations can be clearly seen.

The maximum velocity distribution is presented in Fig. 5.10. The U_{max} values for $2a/\lambda = 0.27$ increase with the increase in Reynolds number. However, tendency of variation of U_{max} is similar in all the cases, as U_{max} becomes largest at $x/\lambda = 0.0$ and 1.0, and smallest at $x/\lambda = 0.5$, as will be expected from the distributions of dimensionless pressure drop, which is discussed in the later sections.

Fig. 5.11 shows the periodicity of flow by plotting U at $y/H = 0.67$ from the central axis, for $2a/\lambda = 0.27$ and Re=40,000, which shows clearly that the flow becomes periodically fully developed after 4^{th} module, as reported by Mendes and Sparrow [70].

5.2.3 Velocity Contours

Fig. 5.12 and 5.13 shows the steady state velocity contours for two different aspect ratios $2a/\lambda = 0.27$ and 0.34 respectively, for three different Reynolds number. It

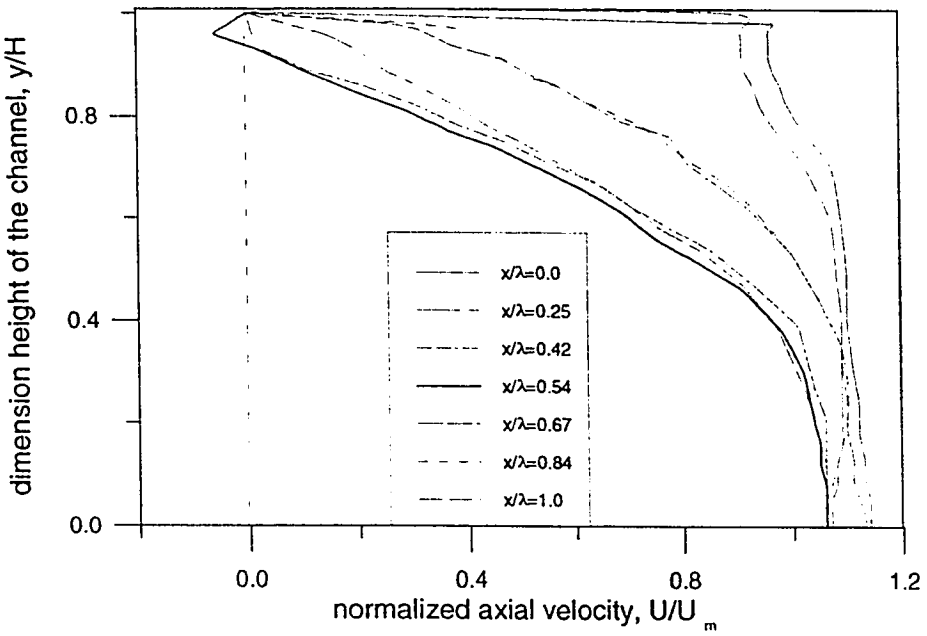

Figure 5.9: Velocity profiles at different locations for $2a/\lambda = 0.27$ and Re=40,000

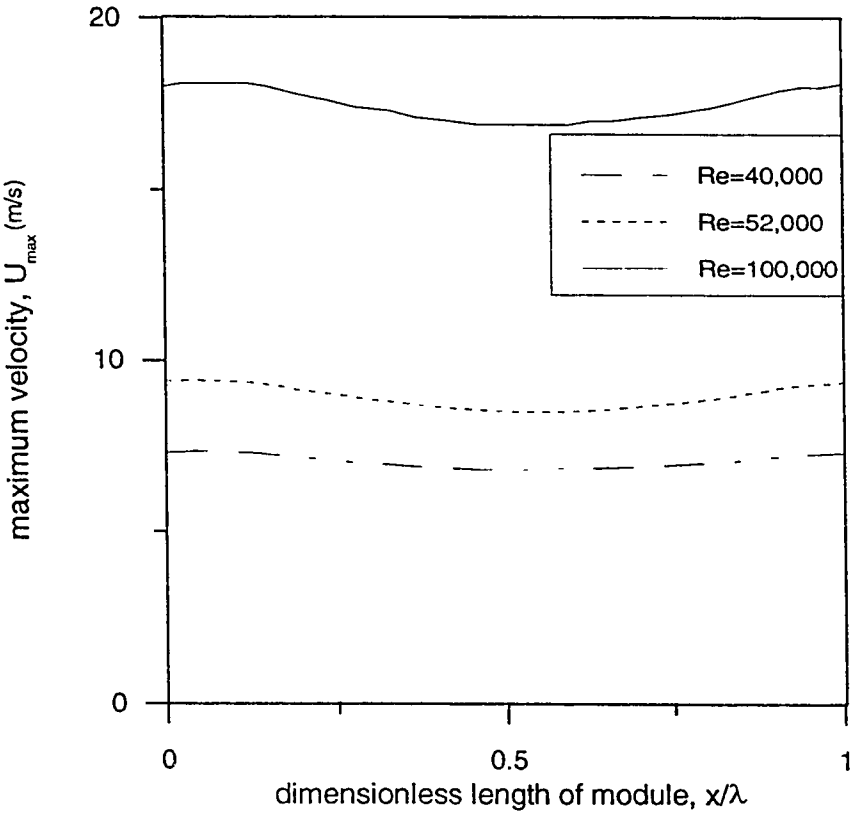

Figure 5.10: Maximum velocity distribution for $2a/\lambda = 0.27$, at different Reynolds number

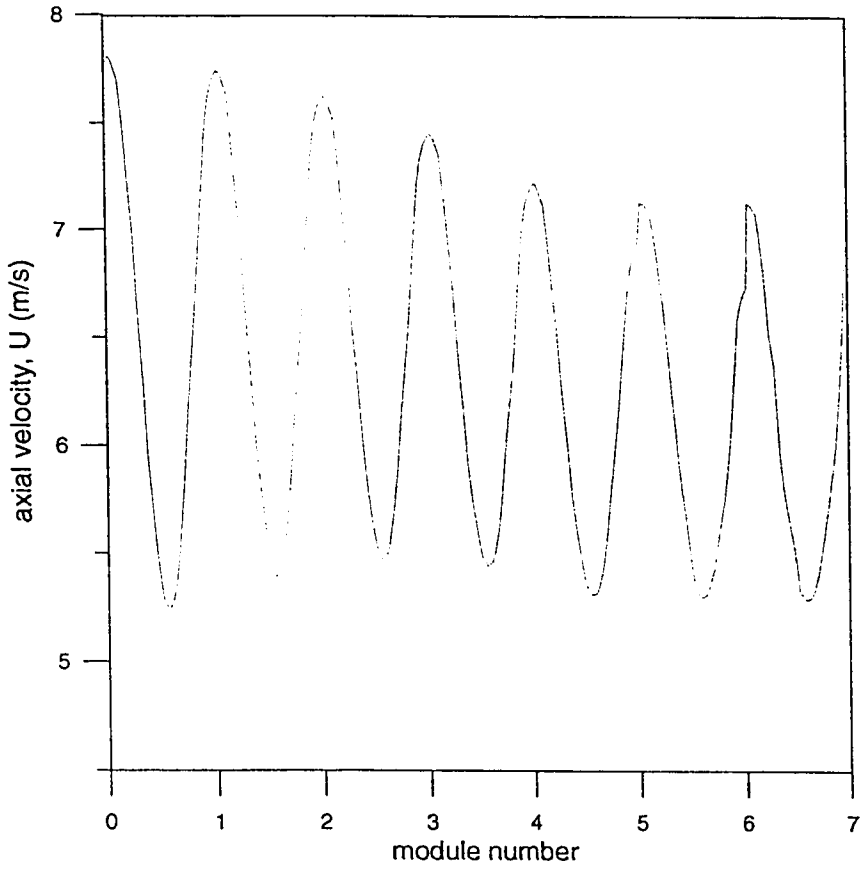

Figure 5.11: Periodic distribution of axial velocity at the symmetric axis, for $2a/\lambda = 0.27$ and Re=40,000

can be seen that the counter-rotating vortices are confined in the furrows along the sinusoidal walls due to high velocity and viscous effects, and are symmetrically located with respect to the central line of the channel.

The effect of Reynolds number on the flow field is also shown, as the Reynolds number increases, the relative strength and size of the recirculation zone grows, where the vortex center is located slightly down-stream from the middle part of the furrow. As the Reynolds number increases, the vortex size increases too and its center shifts slightly downstream. These are similar to the results by Nishimura [57, 78]. As Reynolds number increases, the region of separation grows from the valley of furrow to the location at which the main flow (i.e the forward flow) reattaches to the surface, the remainder of the front-facing facet is washed by a forward flow.

The aforementioned backflow is indicative of flow separation which occurs at a furrow peak because the fluid is unable to turn sufficiently sharply to follow the surface contours.

The effect of aspect ratio can be seen in Fig. 5.12 and 5.13, as the aspect ratio increases, recirculations increases too, for the same Reynolds number. The thickness of the separated region increases with increase in amplitude of the sinusoidally furrowed channel, and for higher amplitude recirculation covers almost whole of the furrow.

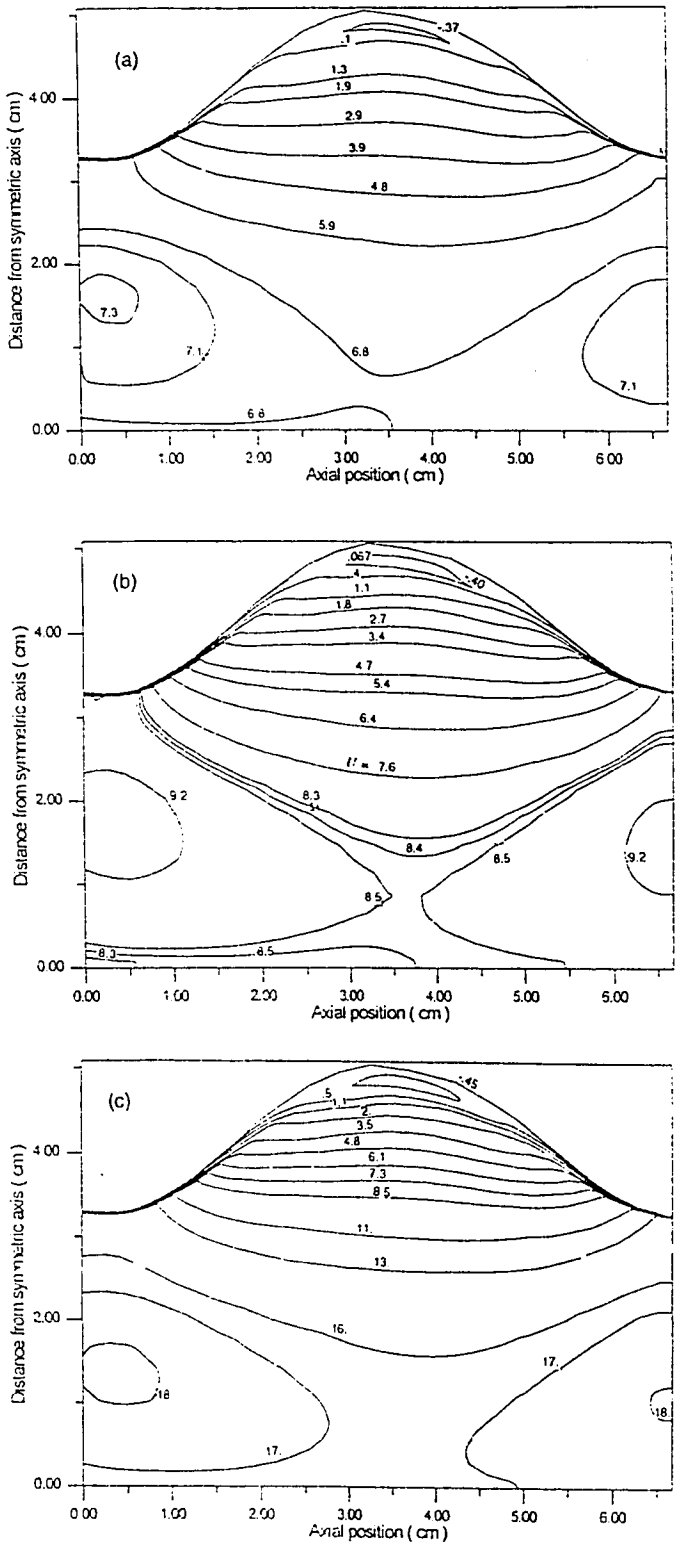

Figure 5.12: Influence of the Reynolds on the axial velocity, $U\ (m/s)$, for $2a/\lambda = 0.27$ (a) Re=40,000 (b) Re=52.000 (c) Re=100.000

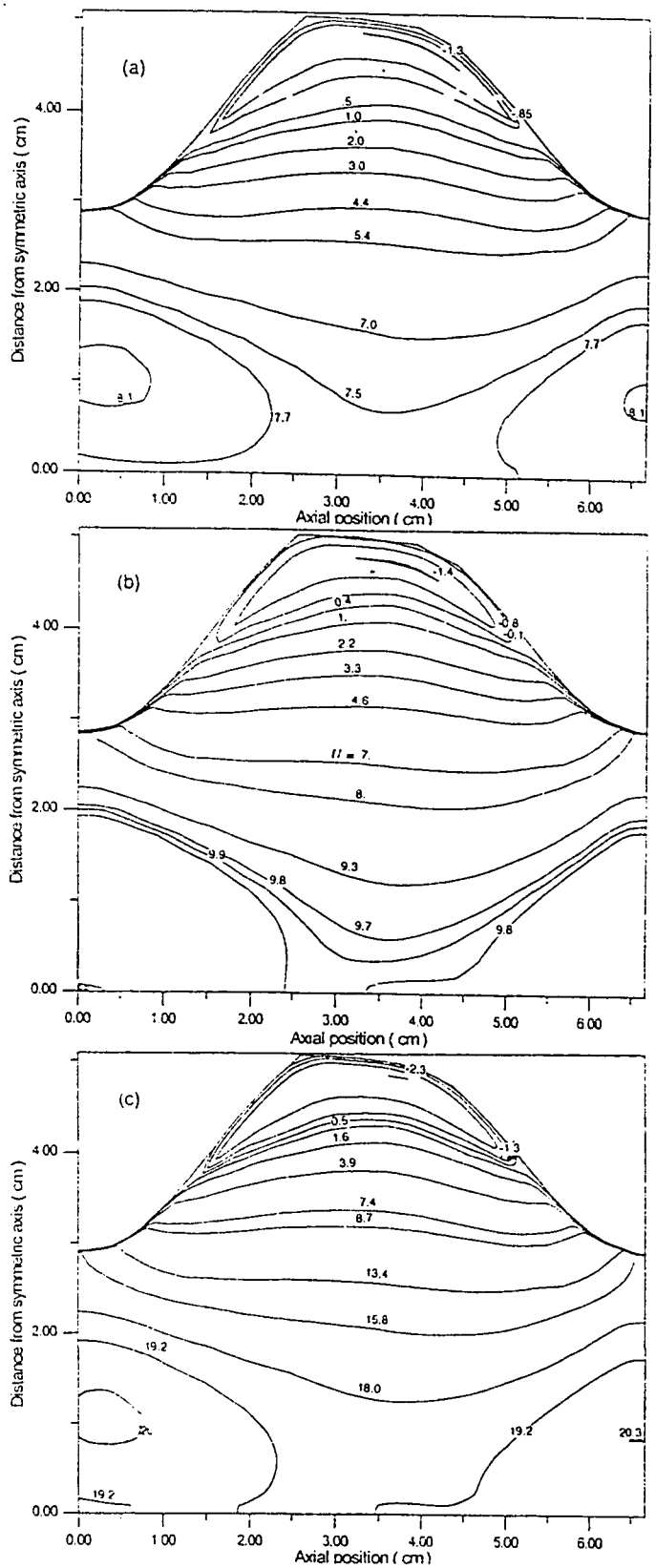

Figure 5.13: Influence of the Re on the axial velocity, U (m/s), for $2a/\lambda = 0.34$ (a) Re=40,000 (b) Re=52,000 (c) Re=100,000

5.2.4 Streamline Contours

The streamlines, which are defined as the lines across which there is zero net flow, are defined as

$$\psi = \frac{\int_H^y \overline{U} y dy - \int_0^x \overline{V} y dx}{\int_H^0 \overline{U} y dy} \tag{5.1}$$

and the streamline contours are shown in Fig. 5.14 and 5.15. Here each streamline extends over the axial length of one cycle and from the channel centerline to the outer boundary of the central part of the channel and stable twin (symmetrical about flow axis) circulated vortices are formed at the maximum cross-section as shown in figures. So convective mixing between the mainstream and the vortex occurs. At larger Reynolds number, the vortex grows and become larger.

5.2.5 Turbulent Kinetic Energy Contours

Distribution of turbulent kinetic energy is shown in Fig. 5.16 and 5.17 reveals that the shear layer, where high gradients of mean velocity occurs, is associated with high turbulent kinetic energy levels. The energy-containing eddies are highly diffusive in the recirculation zone. They are also convected by the slow mean motion and eventually dissipated into heat. Further downstream the turbulence intensity is smaller and should generally show a trend to isotropy [85]. Thus the maximum

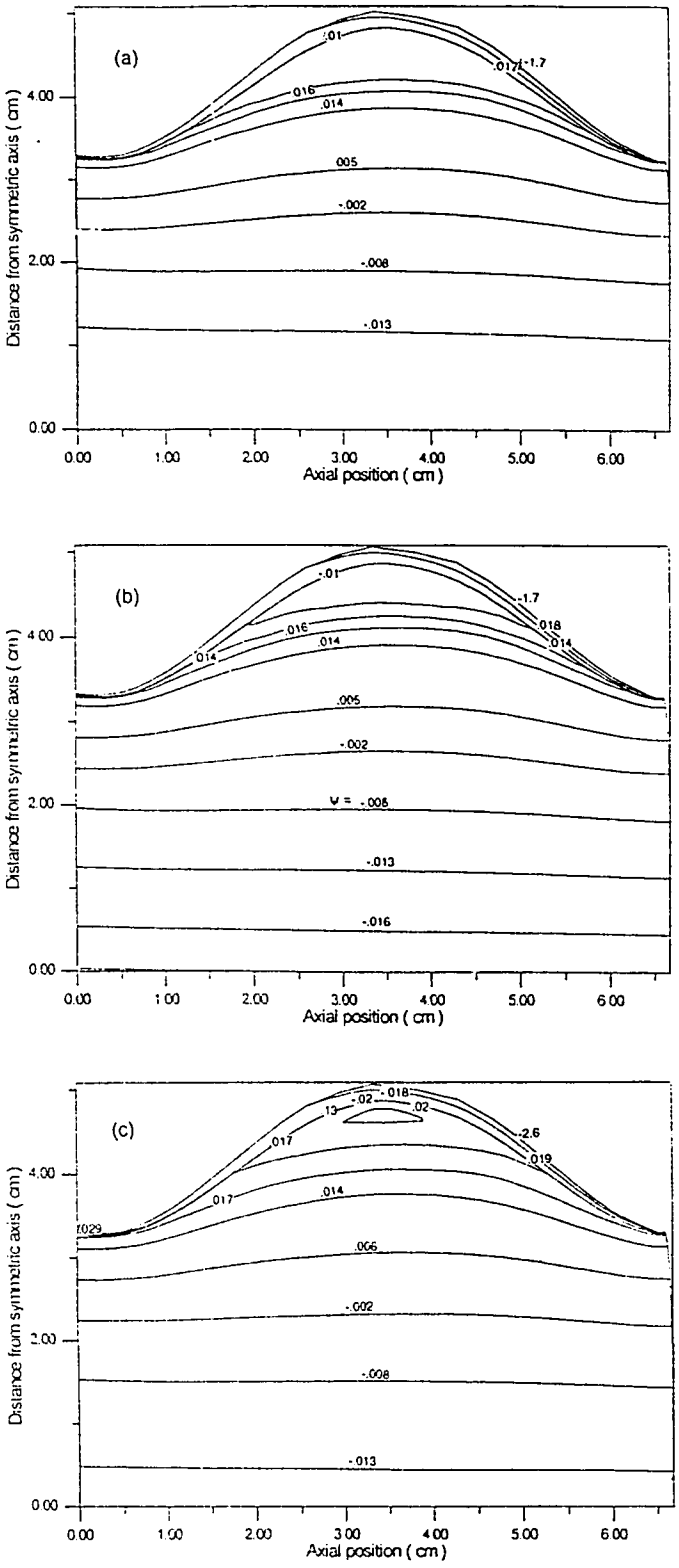

Figure 5.14: Influence of the Re on the stream function, ψ, for $2a/\lambda = 0.27$ (a) Re=40,000 (b) Re=52,000 (c) Re=100,000

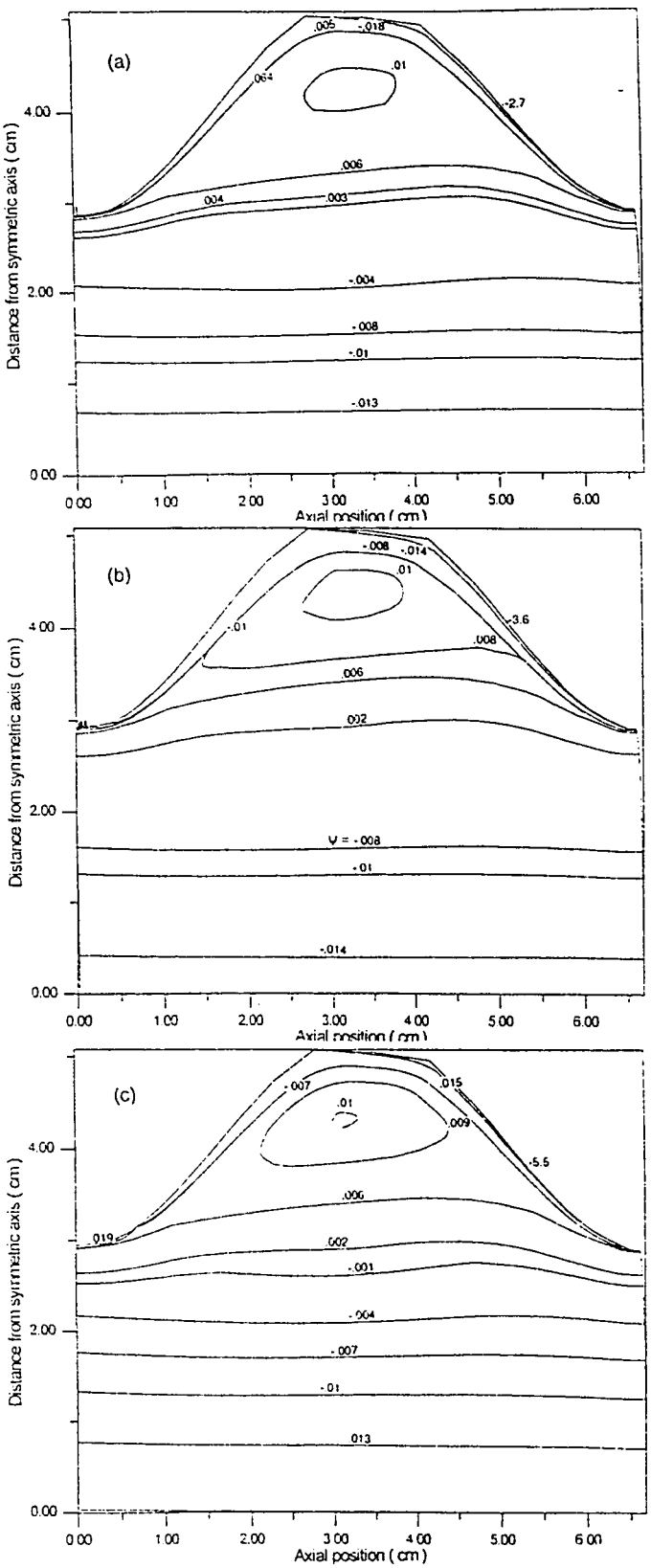

Figure 5.15: Influence of the Re on the stream function, ψ, for $2a/\lambda = 0.34$ (a) Re=40,000 (b) Re=52,000 (c) Re=100,000

turbulent kinetic energy follows the dividing streamline, where strong production of turbulence is expected.

The contours clearly indicate the diffusion towards the centerline, with the location of maximum production of turbulence near the recirculation zone in the upstream region and closer to the centerline in the downstream region.

5.3 Pressure Drop

The results of fully developed pressure for turbulent flow in periodically converging-diverging channel have been determined from the numerical solutions for different values of Reynolds number, and the aspect ratio. Fig. 5.18 shows the dimensionless pressure drop, $(p - p_o)/(\frac{1}{2}\rho U_m^2)$ for the sixth module. Where p is the pressure at centerline, p_o is the reference pressure at $x/\lambda = 0.0$, and U_m is the mean velocity. The peak of the sinusoidal wall is located at $x/\lambda = 0.5$. Consequently, the pressure drop at $x/\lambda = 1.0$ describes the pressure loss per cycle wave of the channel. It can be seen that as the channel diverges pressure drop with its peak slightly downstream from the peak ($x/\lambda = 0.5$) of the furrow, where there is maximum recirculation, as discussed in earlier section. Similar results were also reported by others also [7, 62, 63, 64, 67].

Increasing the Reynolds number, pressure gradient increases and also the pressure drop. The magnitude of pressure drop is markedly effected by the increase

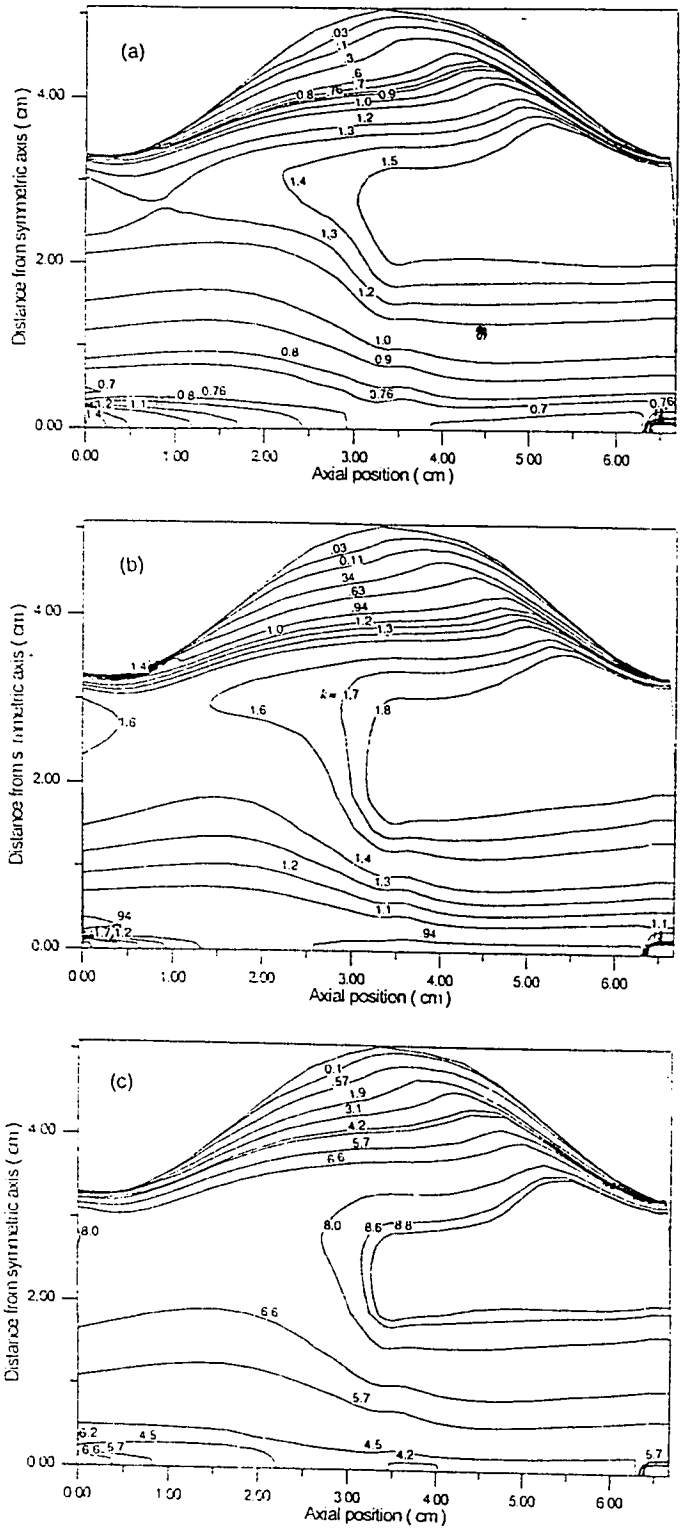

Figure 5.16: Influence of the Re on the kinetic energy, k (m^2/s^2), for $2a/\lambda = 0.27$ (a) Re=40,000 (b) Re=52,000 (c) Re=100,000

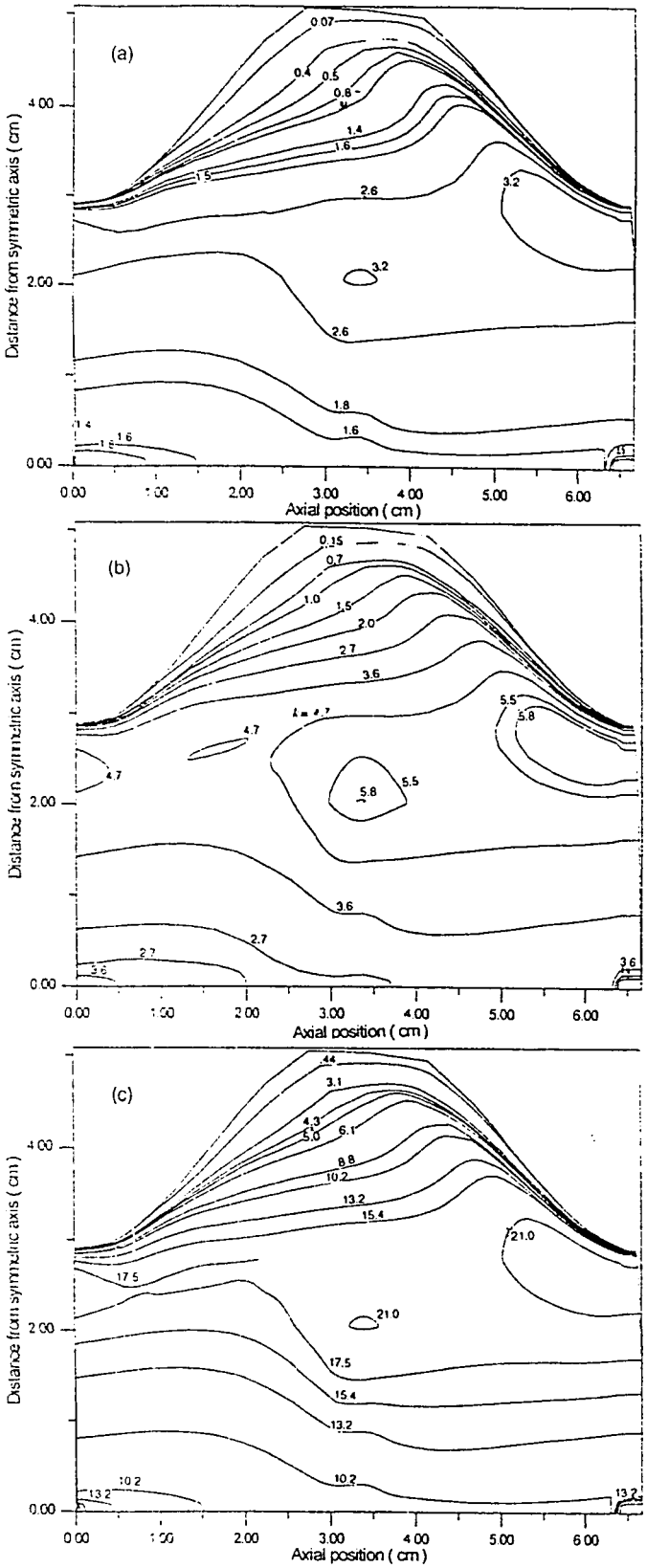

Figure 5.17: Influence of the Re on the kinetic energy, k (m^2/s^2), for $2a/\lambda = 0.34$ (a) Re=40,000 (b) Re=52,000 (c) Re=100,000

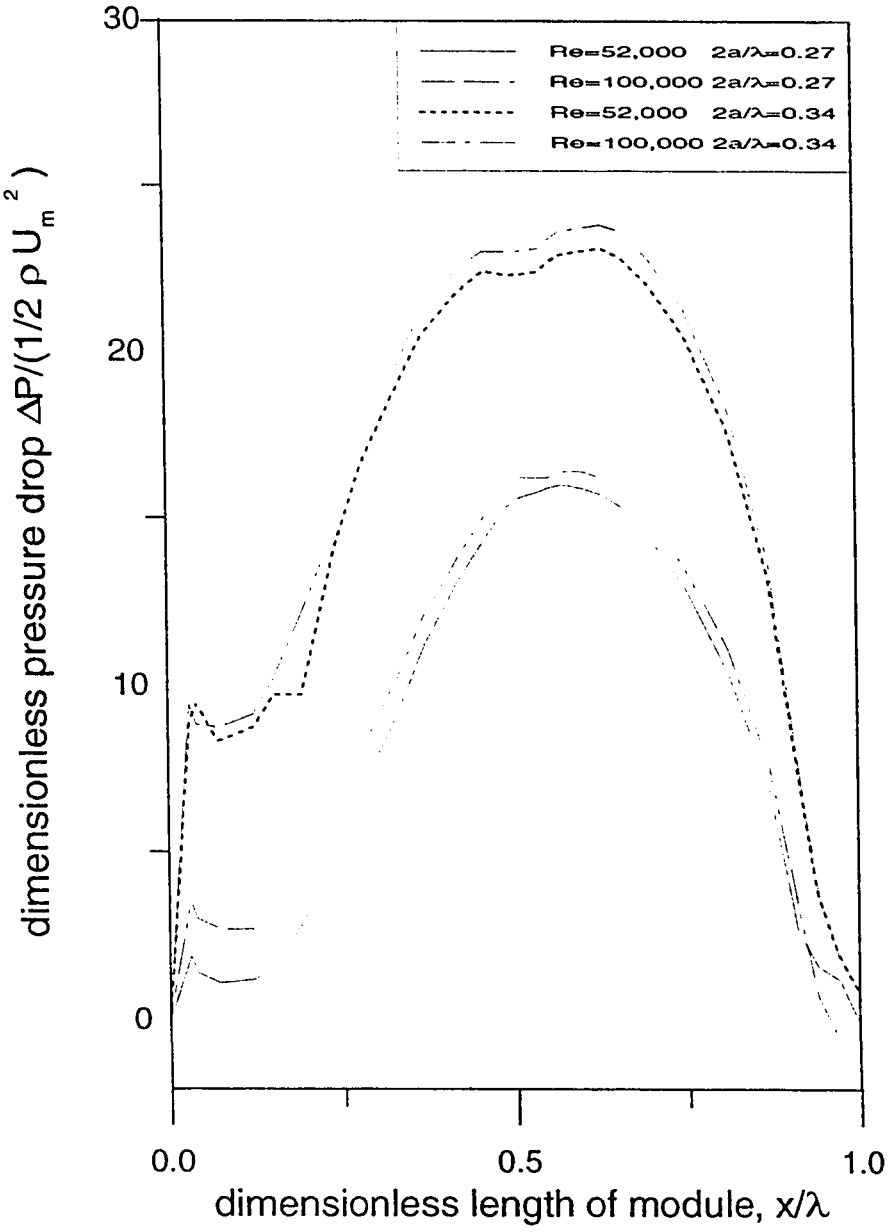

Figure 5.18: Streamwise distribution of pressure

in channel amplitude (or aspect ratio). Larger the difference between maximum and minimum height of the channel, larger the changes velocity and increase the propensity towards the flow separation, which causes larger pressure drop, as Fig. 5.18 shows, for the same Reynolds number (Re=40.000). When the aspect ratio increases from 0.27 to 0.34, the pressure drop increases by nearly 40%. Here, it can be seen that initially pressure drop increase suddenly as the flow enters in the module, this is because of the fact that at the inlet as area is smallest, velocity increases causing drop in pressure. Further downstream pressure drop decrease and start increasing gradually as channel diverges.

Fig. 5.19 shows the dimensionless pressure drop due to each module, which starts increasing with the module, and the gradient reduces as the flow become developed. This also shows that pressure drop increases with Reynolds number and also with the increase in aspect ratio. The comparison between the numerical and experimental pressure drop with increase in Reynolds number is shown in Fig. 5.20 for $2a/\lambda = 0.27$, shows good agreement. Some error may be due to mathematical formulation or due to the model used. Fig. 5.21 shows the drop in pressure per module for two different aspect ratios at the same Reynolds number (Re=40,000). The pressure drops significantly upto fourth module and after that it becomes almost insignificant.

The relatively large pressure drops for periodically converging-diverging channel is not proportionate with regard to the attainment of a favorable trade-off between

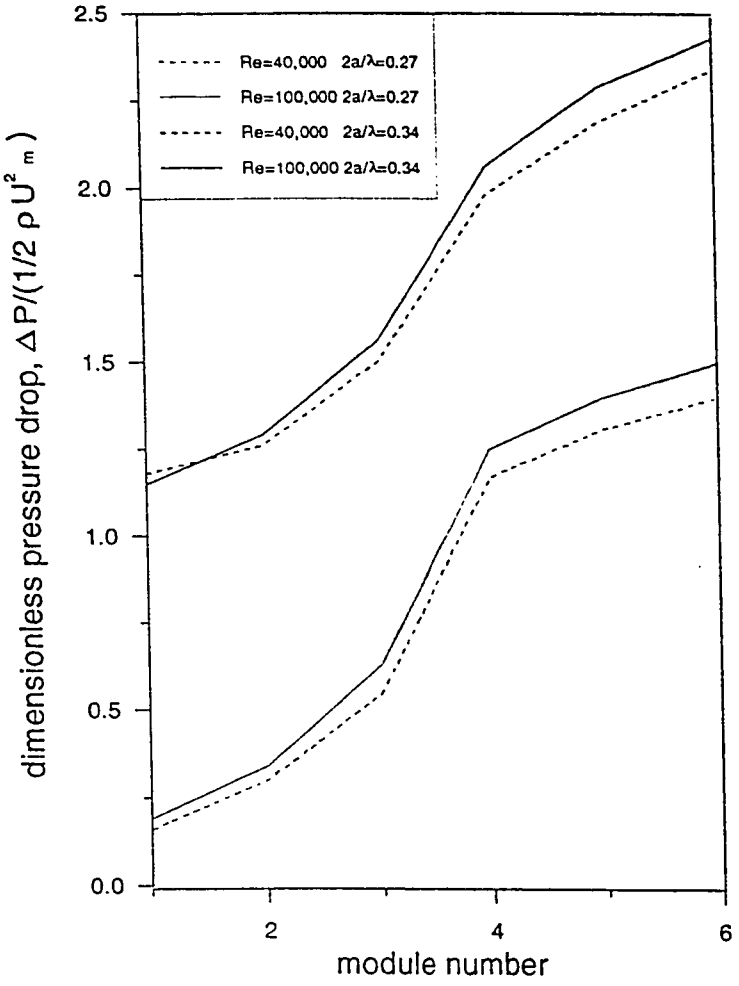

Figure 5.19: Dimensionless pressure drop as a function of module number

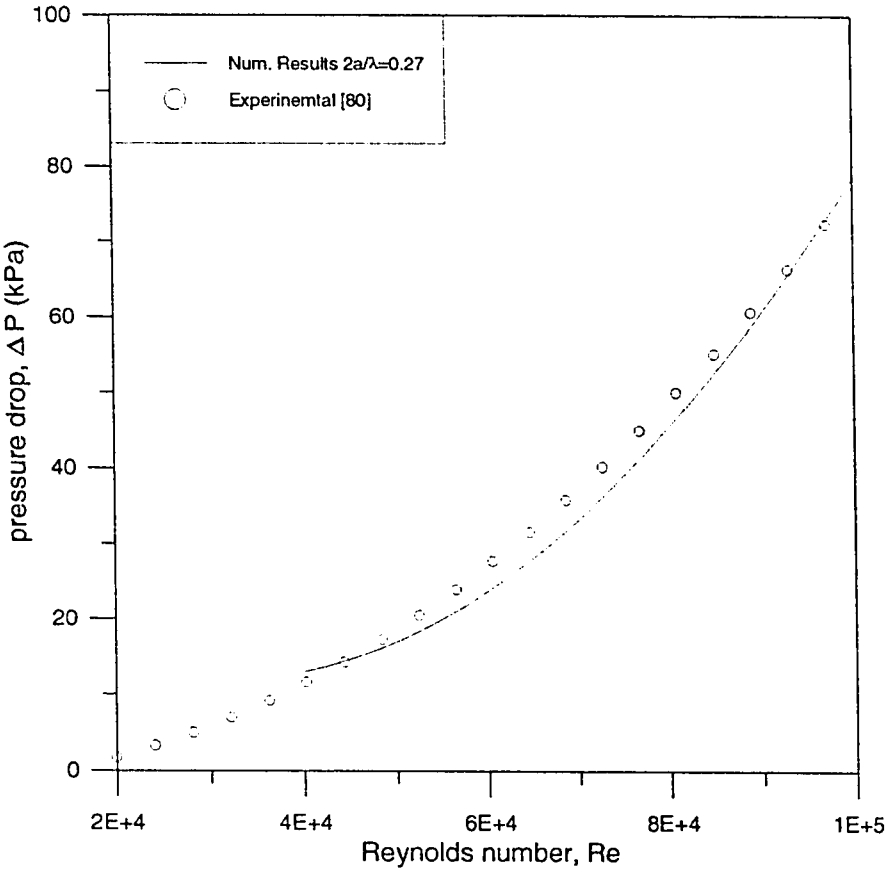

Figure 5.20: Pressure drop versus Reynolds number for Re=40,000

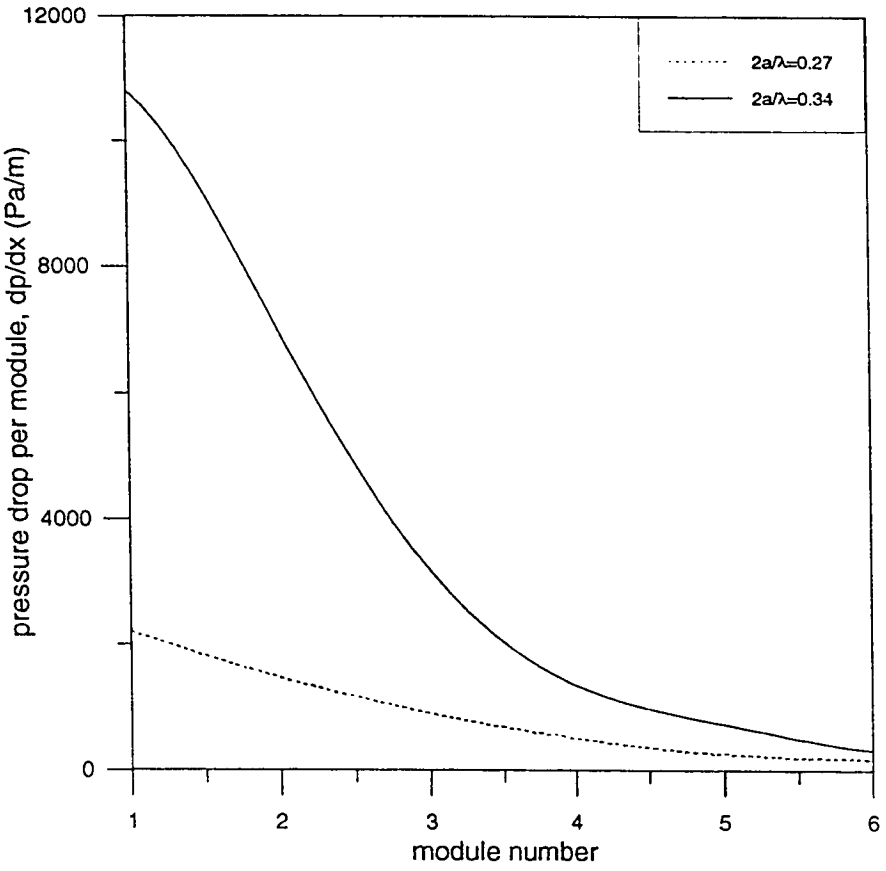

Figure 5.21: Pressure drop per module at Re=40.000 for different aspect ratios

heat transfer enhancement and pressure drop (pumping power) penalty, listed by Sparrow and Prata [50], and detailed comparison is given by Asako et al. [38].

5.3.1 Friction Factor

The friction factor f is determined by [62]

$$f = -\frac{(\frac{dp}{dx})D_H}{\frac{1}{2}\rho U_m^2} \tag{5.2}$$

where dp/dx is the pressure gradient determined by the pressure drop in a module. Thus the determined friction factors are plotted in Fig. 5.22 as a function of Reynolds number for $2a/\lambda = 0.27$ and Re=40,000, and are compared with experimental data and also with a channel of straight walls [80]. Initially f falls as Reynolds number increase (up Re=50,000), and then f becomes nearly constant. It is noteworthy to observe that the friction factor of a converging-diverging channel is higher than that of straight channel. Similar trend is also reported by Amano [29] and Asako et al. [24]. It is also clear that careful optimization of the geometric parameters is needed in order to avoid excessive pressure drops.

5.4 Heat Transfer

The presentation of results will begin with the fully developed heat transfer coefficients and Nusselt numbers.

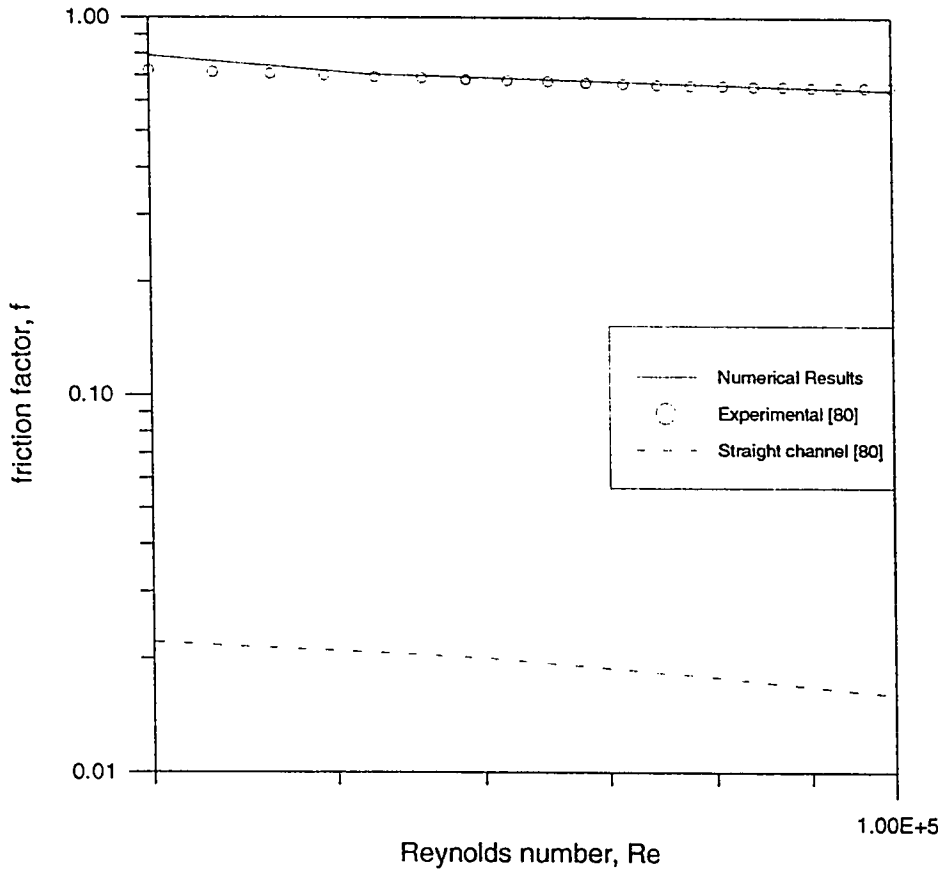

Figure 5.22: Friction factor as a function of Reynolds number for $2a/\lambda$=0.27

5.4.1 Fully-Developed Nusselt numbers

The evaluation of the fully developed heat transfer coefficient is calculated by:

$$h_x = \frac{q_c''}{(T_w - T_b)} \tag{5.3}$$

and the average heat transfer coefficients were obtained by the integration of the local heat transfer coefficients:

$$h_a = \int_0^L \frac{h_x dx}{L_c} \tag{5.4}$$

The average Nusselt number of channel can be written as [44];

$$Nu = \frac{hD_H}{k} \tag{5.5}$$

Predicted local and overall Nusselt numbers provides an indication of heat transfer characteristics irrespective of channel size. These are presented along the channel walls in order to investigate the local and overall heat transfer characteristics as affected by geometric parameters, Reynolds number and swirl number. The present computational capabilities are only able to treat successfully some of the simpler limiting cases of the present problems. The distribution of the computed local Nusselt number for Re=40.000. for two different aspect ratios of 0.27 and 0.34 is shown and compared with experiments in Fig. 5.23 and 5.24. The major difference among the two Nusselt number distribution is more pronounced among the last four or

five modules, and having good agreement with experimental results [80]. Temperature patterns and, therefore, local Nusselt number distributions are similar for both Reynolds numbers as Fig. 5.25 shows. However, the magnitudes (i.e, occurring of the maxima and minima for each Reynolds number and for each module) are different.

The effects of aspect ratios on local Nusselt number can also be seen from Fig. 5.26 and 5.27, for a different Reynolds number. These numerical calculations show good agreement with the results obtained by Sanici and Dini [80]. Similar distribution is also found in the numerical solution of converging-diverging channel by Grag et al. [44] and Sano et al. [67]. It is also observed that the local Nusselt number increase, with increase in pressure drop, and decrease when pressure drop decrease.

Fig. 5.26 and 5.27 show that higher Reynolds number shifts the local Nusselt number distribution up considerably, it is due to the increase in velocity. Doubling the Reynolds number almost double the magnitude of the Nusselt number distribution.

5.4.2 Maximum Heat-Transfer coefficient

In general, the data for heat-transfer at the reattachment point are treated by using the velocity of separated layer and the distance from the separated point to the reattachment point of flow as the reference velocity and length [86].

The occurrence of the maximum pressure and maximum heat transfer is almost

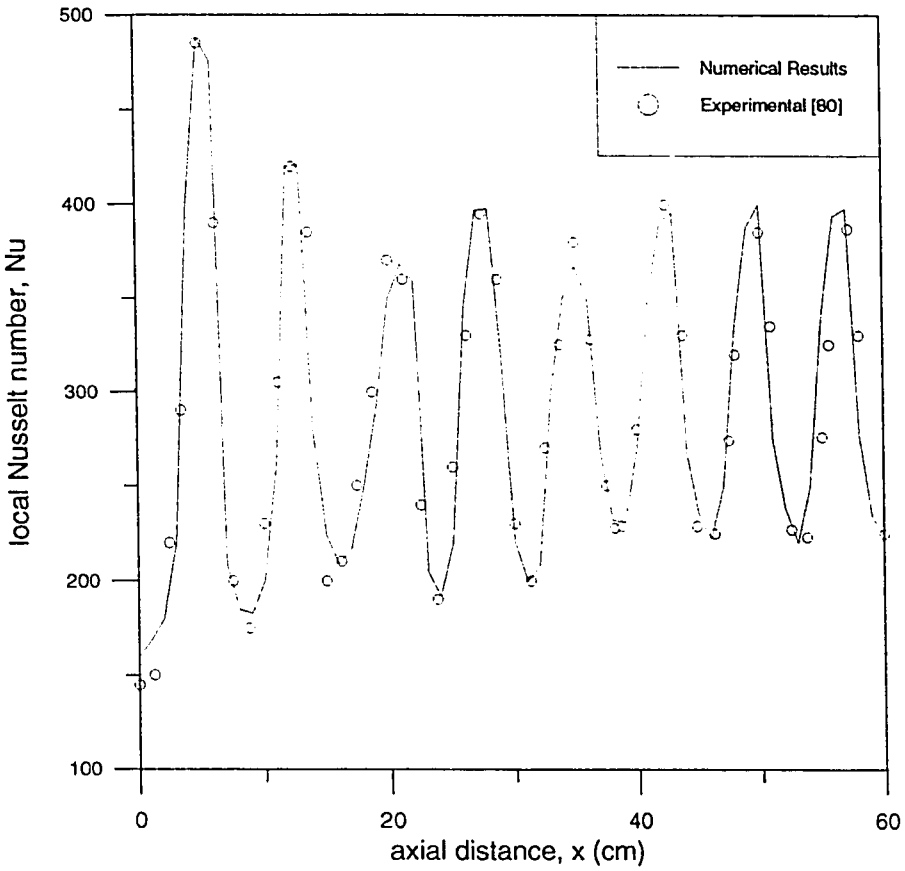

Figure 5.23: Local Nusselt number distribution for $2a/\lambda$=0.27 and Re=40,000

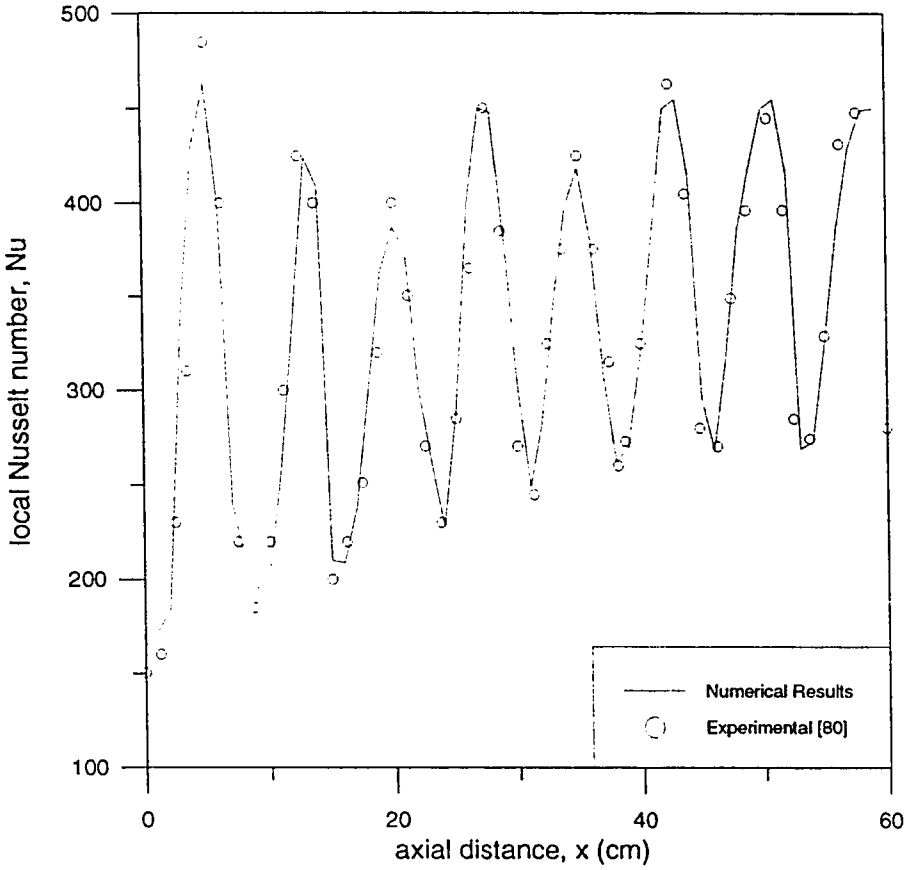

Figure 5.24: Local Nusselt number distribution for $2a/\lambda$=0.34 and Re=40,000

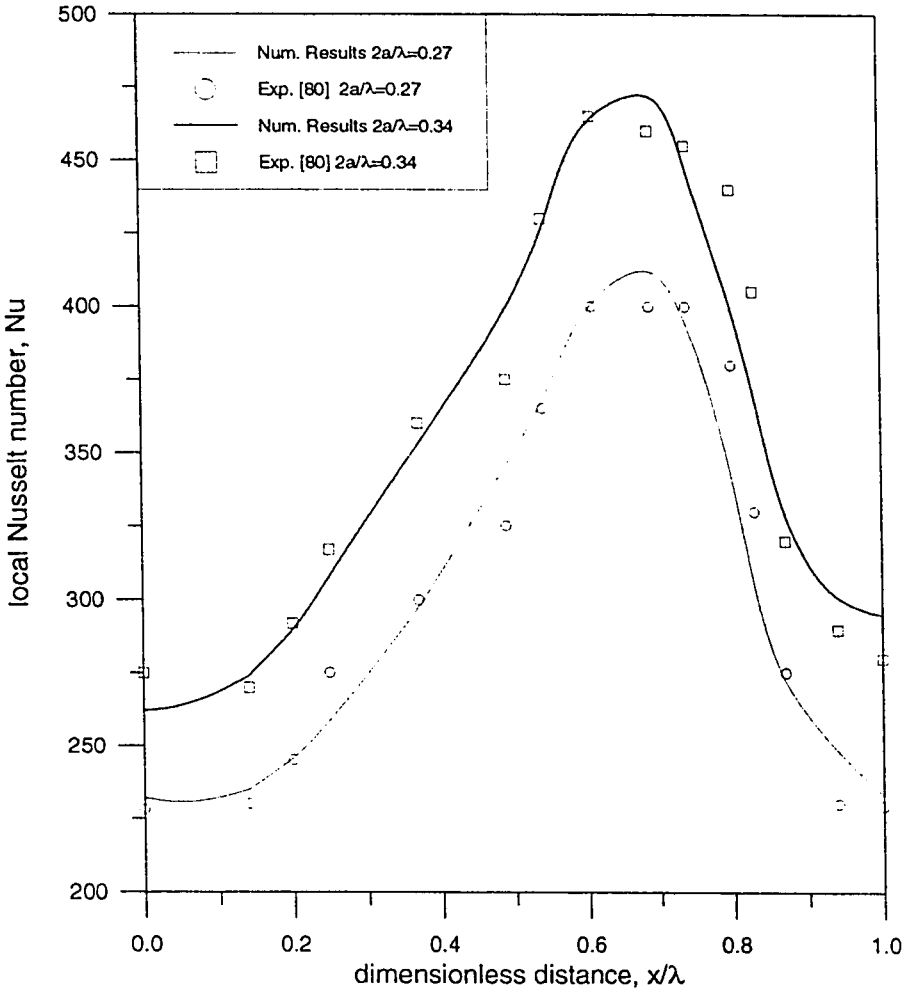

Figure 5.25: Streamwise distribution of local Nusselt number for Re=40,000

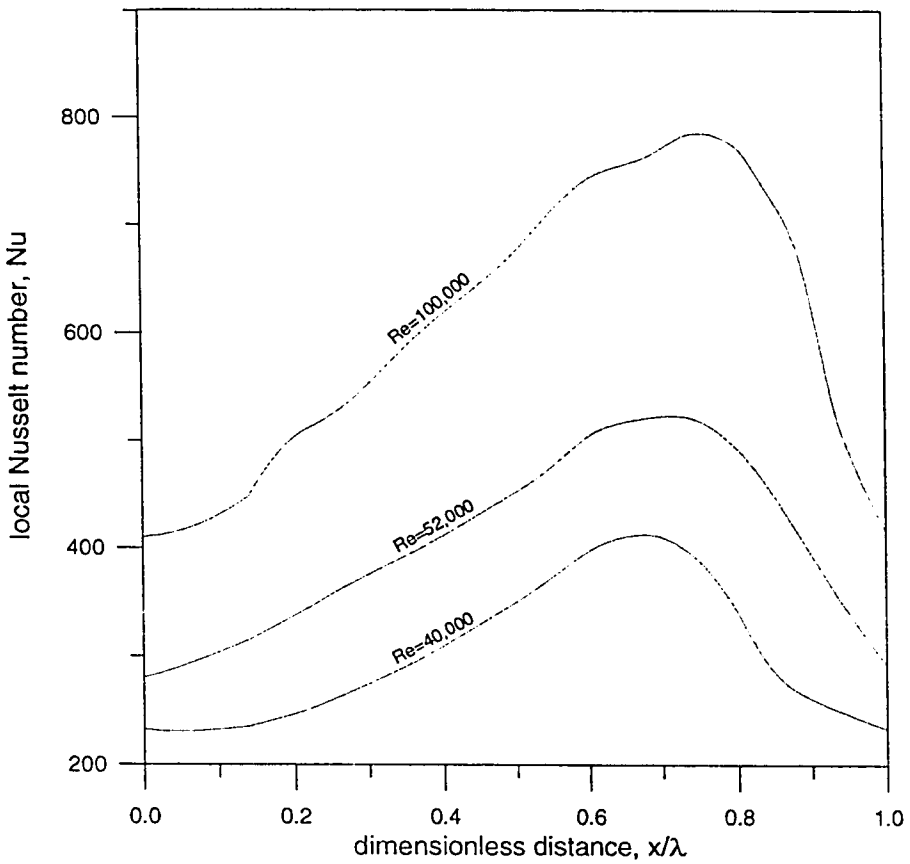

Figure 5.26: Variation of Nusselt number with x/λ for $2a/\lambda = 0.27$

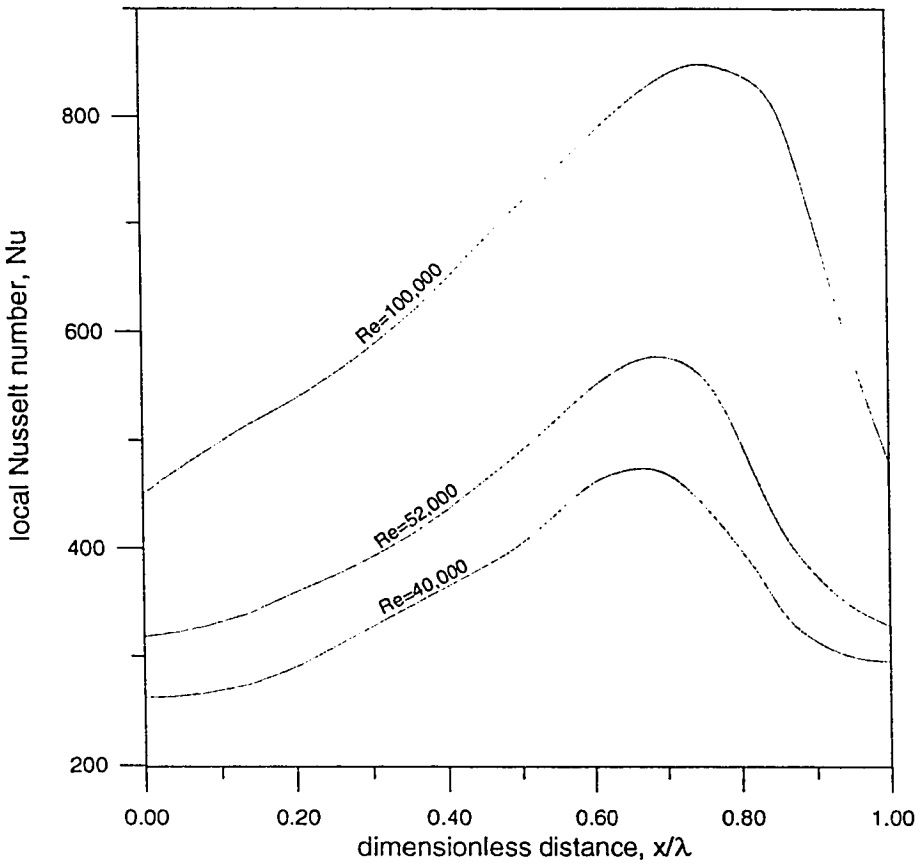

Figure 5.27: Variation of Nusselt number with x/λ for $2a/\lambda = 0.34$

at the same location in the channel. On the other hand, the velocity of the separated layer depends upon the aspect ratio of the channel. The relation of maximum Nusselt number, Nu_{max} and Reynolds number is presented for two aspect ratios in Fig. 5.28.

The correlation for maximum Nusselt number with Reynolds number is given by (Pr is constant throughout the calculations);

$$Nu_{max} = CRe^{0.69} \tag{5.6}$$

Here the constant C depends upon the aspect ratio and is given in the Fig. 5.28

5.4.3 Average Nusselt Number

Average Nusselt number as a function of Reynolds number is shown in Fig. 5.29, for two different geometries. Experimental data of Oyakawa et al. [62] is used for comparison with the present computational method, also compared with average Nusselt number distribution for straight channel. The geometry considered by Oyakawa et al., uses wavy sinusoidal channel which has width, $W = 20mm$, wavelength, $\lambda = 80mm$, and 12.5 wavelength long. The experimental data of computed average Nusselt number, Nu_{avg} get closer to the one measured by Oyakawa et al. [62] But the discrepancy is mainly due to the differences in the channel's geometry. Comparison to theoretical, fully developed flat channel results shows significant augmentation [65].

Fully developed average Nusselt number, as seen in the figure, for the overall

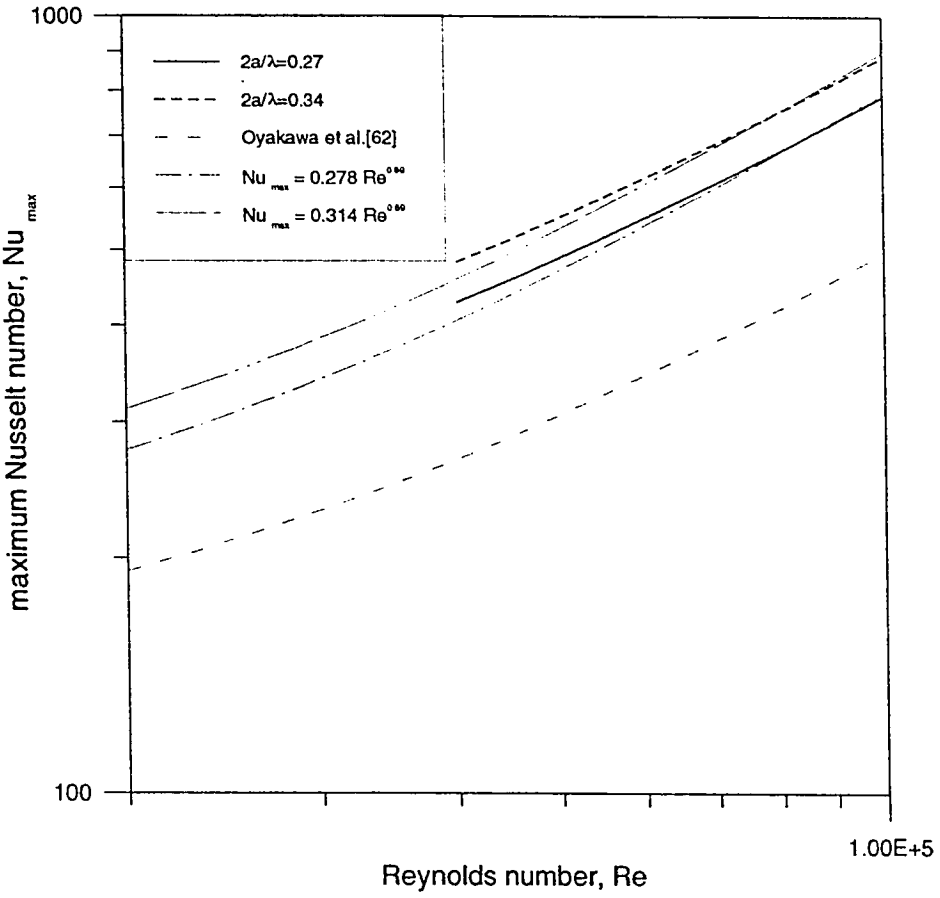

Figure 5.28: Variation in maximum Nusselt numbers with Reynolds number

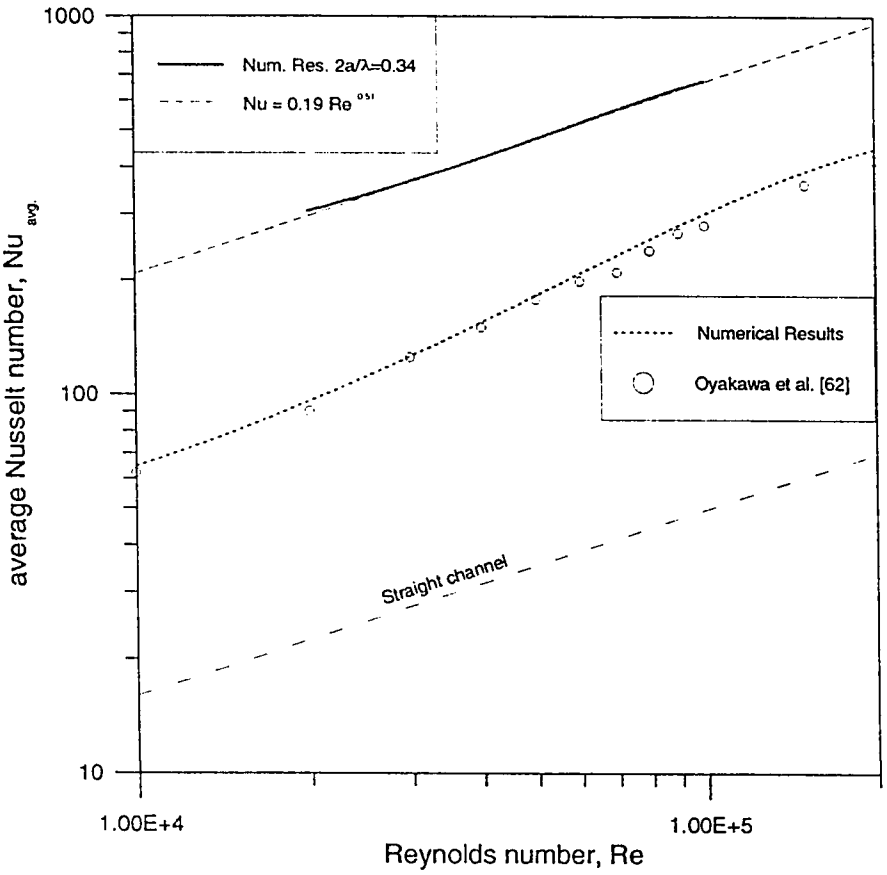

Figure 5.29: Variation in average Nusselt number with Reynolds number

range of Reynolds number extends from about 10,000 and 200,000. The correlation for average Nusselt number with Reynolds number is given by;

$$Nu = 0.19Re^{0.51} \tag{5.7}$$

This equation is also plotted in Fig. 5.29, where it is seen that there is only very slight data scatter relative to the line. The value of 0.51 of the Reynolds number exponent is lower compared to 0.8 for a standard turbulent duct-flow situation. This is not unexpected, since the wavy-channel flow contains large zones of recirculation, not present in conventional ducts.

5.5 Swirling Flow and its Effects

Swirling flow in a channel is a complex phenomena, it possess several distinctly different flow regimes, either one or two recirculation regions, extremely high levels of turbulence, and periodic asymmetries under same conditions. Separated recirculating flow which established downstream of swirling vanes has been commonly used to allow the stabilization of high intensity turbulent flames in industrial processes [87]. There are many interesting phenomena in the flow field with the introduction of swirl [88]. Among these is an increase in growth rate entrainment, and decay of the core flow just downstream of the expansion. Consequently, the flow reattachment zone moves upstream as swirl strength is increased. Swirl is also responsible

for increased shear rates, greater turbulence production, and longer path lengths for a particular fluid particle so that the effect of swirl, like the effect of recirculation, is also to increase Nusselt number significantly over those found in purely axial channel flow. Due to swirl, the production of turbulent energy is suppressed in the vicinity of the inner wall where the radial gradient of angular momentum is positive and enhanced near the outer wall where this gradient is negative. The differences in turbulent energy production imply variation in rate of growth of the boundary layers and their ability to sustain streamwise pressure gradients.

A further complex phenomena which frequently occurs in swirling flow is the development of an unsteady (although usually periodic) axisymmetric in the flow field. For the swirling inlet flow , an additional radial pressure gradient is established across the passage to balance the centrifugal force acting on the through flow [89]. Thus, with this swirling velocity component, the flow is pressed towards the wall by the centrifugal force and the wall boundary layer is less likely to separate. However, excessive amounts of swirl reduces the axial velocity too far near the inner wall of the diffuser or induces a reversed flow region, which again results in high heat transfer rate.

5.5.1 Calculations of Flow Field with Swirl

Results for swirling flow indicates that the channel with expansions and contractions is accompanied by a region of separation close to the wall. This separation causes

an augmentation of the heat transfer coefficient. Increase in swirl number causes a reduction in the separation region as shown in Fig. 5.30.

The above mentioned figure allows the comparison of an axial velocity contours for the various swirl intensities. With no swirl, the flow separates in the expanding section along the outer wall. As the swirl component is increased, the flow is pressed towards the wall and the boundary-layer development and the flow separation along the diffuser wall is suppressed. However, for increased swirl, a solid vortex core starts developing, creating a low-pressure near the wall, a stagnation or back flow region is formed there and thus, the effective area for pressure rise is decreased, Fig. 5.30 also shows that with increasing swirl number the highest axial velocities moves towards the core.

5.5.2 Effects of Swirl on Heat Transfer

As the swirl number increases, local Nusselt number increases, this is due to the suppression of the recirculation zone, as discussed earlier and is a direct result of the shortening reattachment length.

The shortening of the recirculation region causes shear rate and hence production of turbulence kinetic energy to increase with consequently higher heat transfer rates. This enhancement is also promoted by higher local mean velocities as the tangential velocity component increases at nominally constant values of mean axial velocity. Effect on distribution of average Nusselt number can be seen in Fig. 5.31, it is

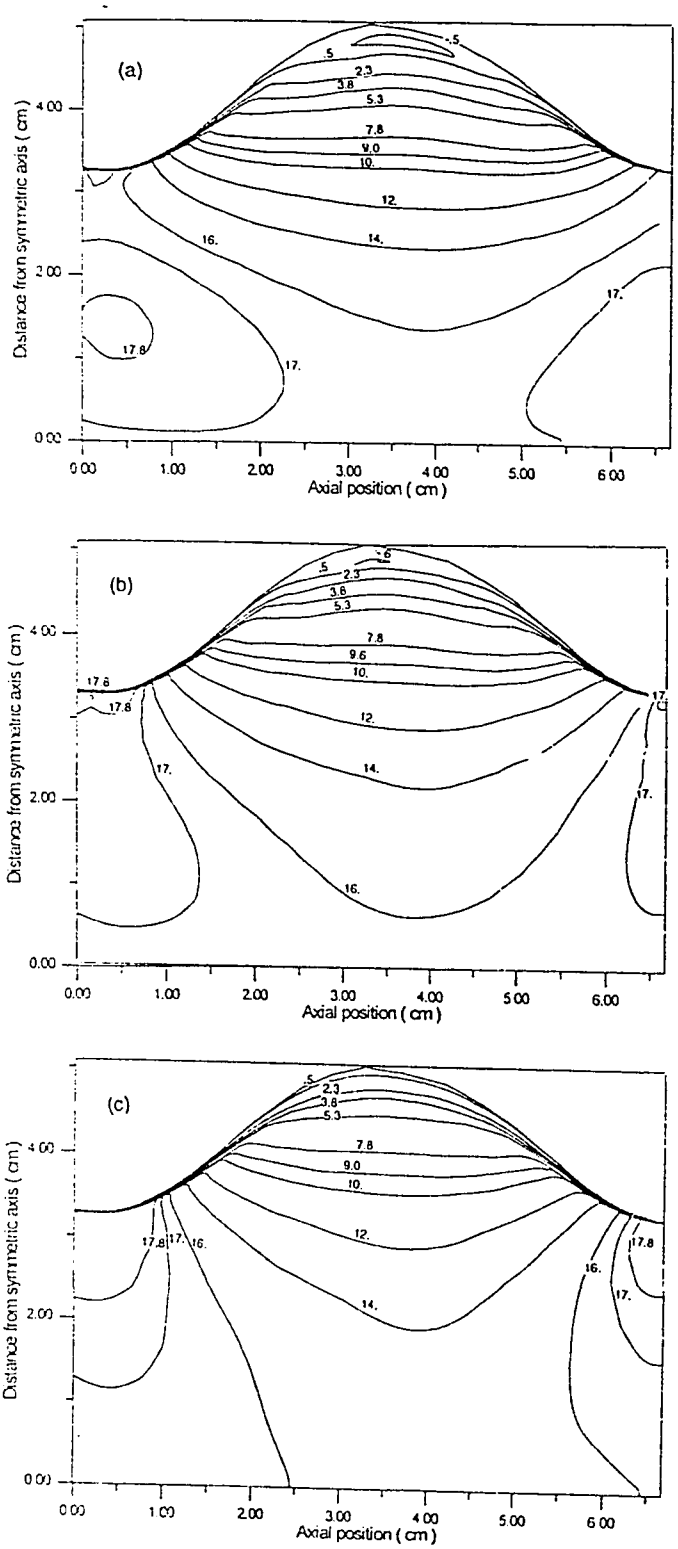

Figure 5.30: The influence of swirl number on the axial velocity, U (m/s), for $2a/\lambda = 0.27$ (a) Swirl No.=0.3, (b) Swirl No.=0.6, (c) Swirl No.=0.9, for Re=40,000

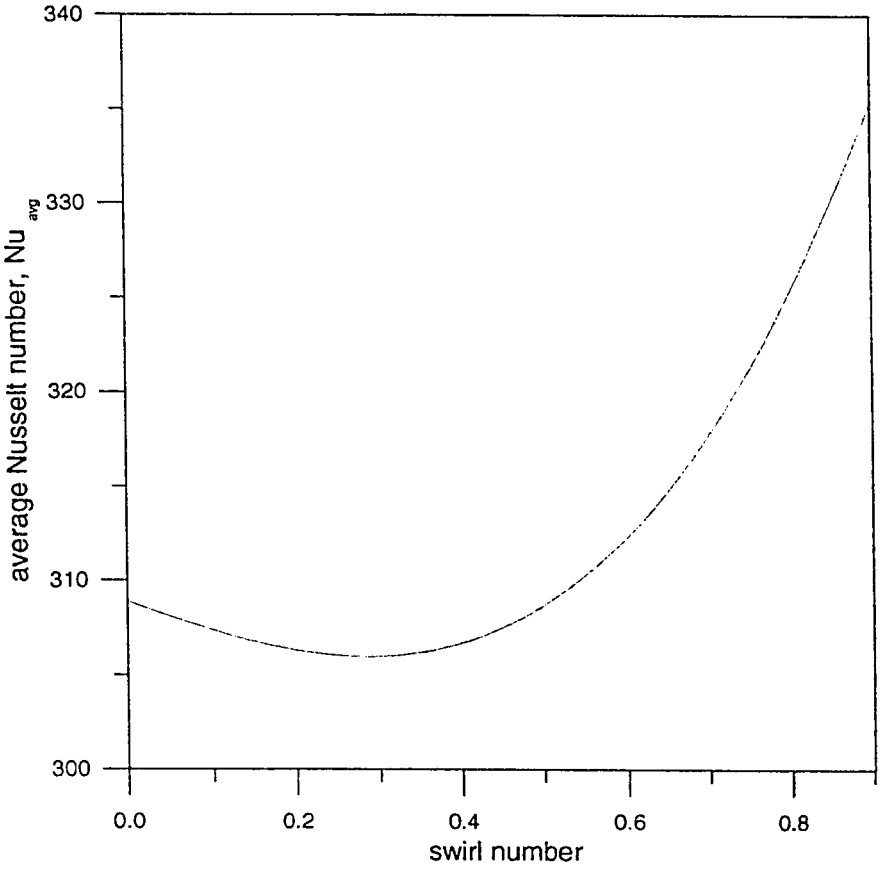

Figure 5.31: Variation in average Nusselt number with swirl number for $2a/\lambda = 0.27$, Re=40,000

observed that as the swirl number increases the Nu_{avg} also increases, almost linearly upto Swirl No. = 0.5, after that Nu_{avg} increases more rapidly than it does before.

Chapter 6

Conclusions

This study, in conjunction with other experimental work proves that the periodically converging-diverging walled channel improves the mechanism responsible for enhanced heat transfer by introducing spatially periodic disturbances to a channel flow. Specifically, it can be seen that periodic contraction and expansion leads to free shear layers, and the flow separates mainly in the diverging portion, but for higher Reynolds number and aspect ratios, it separates in the converging portion as well.

The present research brings together seemingly for the first time, the experimental and computational results for the periodic fully developed regime in a channel with periodically varying cross-sectional area, with good agreement between the two sets of results.

The main results obtained in this study can be summarized as follows:

1) The maximum separation occurs in the region x/λ =0.2 to 0.6 in almost all the cases.

2) The pressure drop per-module and friction factor for the converging-diverging channel is greater than that of the straight channel.

3) The per-cycle pressure drop in the fully developed region is constant for each cycle and increases with Re (3 to 4%) and $2a/\lambda$ (40 to 50%).

4) The distribution of the local Nusselt number and pressure drop are related in such a way that Nusselt number increases with the increase in pressure drop, with their peaks almost at the same location in a module.

5) As the aspect ratio ($2a/\lambda$) increases, an increase in heat transfer by around 15% is observed. This can also be recognized with accompanying large pressure drops.

6) Increase in local Nusselt number is around 16% per 10.000 increase in Reynolds number.

7) The average Nusselt number can be correlated with a power-law representation, $Nu_{avg} = 0.19Re^{0.51}$, resulted in Re exponent of 0.51, which agrees quite well with exponents used for forced convection, which have similar periodic-separation and high turbulence levels. Nu_{avg} varies cyclically and increase with the Reynolds number.

8) The maximum Nusselt number can also be correlated with Reynolds number by $Nu_{max} = CRe^{0.69}$, where C is a constant that varies with aspect ratio.

9) The results show that the increase in the swirl number causes a reduction in the separation and increase the heat transfer (is about 6% per 0.3 increase in swirl number), by increasing the rate of mixing.

10) The results obtained using the $k - \varepsilon$ turbulence model show that the heat transfer rates are in good agreement with the experimental results.

11) The above conclusions generally support the broad correctness of the near-wall turbulence model that has formed the basis for the calculations.

12) The important observation is that increase in aspect ratio ($2a/\lambda$), causes 40% increase in pressure drop, where increase in local heat transfer is only around 15%. Thus, one has to compromise between the pressure drop and heat transfer while designing a heat exchanging device.

Bibliography

[1] Rodi, W., *Turbulence Model and their Application in Hydraulics. A State of the Art Review*, International Association for hydraulic Research, University of Karlsruhe, Karlsruhe. FRG, 2nd Edition, (1984)

[2] Cho, H.H., and Goldstein, R.J., *An Improved Low-Reynolds-Number k-ε Turbulence Model for Recirculating Flows*, Int. Jr. Heat Mass Transfer, Vol. 37, No. 10, pp. 1495-1508, (1994)

[3] Goldstein, L., and Sparrow, E.M., *Heat/Mass Transfer Characteristics for flow in a Corrugated wall Channel*. Jr. of Heat Transfer, Vol. 99, pp. 187-194, (1977)

[4] Mendes, P.S., and Sparrow, E.M., *Periodically Converging-Diverging Tubes and their Turbulent Heat Transfer, Pressure Drop, Fluid Flow and Enhancement Characteristics*. Jr. of Heat Transfer, Vol. 106, pp. 55-63, (1984)

[5] Nishimura, T., Yoshino, T., and Kawamura, Y., *Numerical Flow Analysis of Pulsatile Flow in a Channel with Symmetric Wavy Walls at Moderate Reynolds*

Number, Jr. of Chem. Engg. of Japan, Vol. 20, No. 5, pp. 479-485, (1987)

[6] Yalamanchili, R.C., *Flow of Non-Newtonian Fluids in Corrugated Channels*, Int. Jr. Non-Linear Mechanics, Vol. 58, No. 5, pp. 535-548, (1993)

[7] Patel, V.C., Chon. J.T. and Yoon, J.Y., *Turbulent Flow in a Channel with a Wavy Wall*, Jr. of Fluids Engg., Vol. 113, pp. 579-586, (1991)

[8] Patankar, S.V., Lin. C.H., and Sparrow, E.M., *Fully Developed Flow and Heat transfer in Duct having Streamwise-Periodic Variations of Cross-Sectional Area*, Jr. of Heat Transfer, Vol. 99, pp. 180-186, (1977)

[9] Gosman, A.D., *Computer Aided Engineering: Heat Transfer and Fluid Flow*, John Wiley and Sons. (1985)

[10] Fletcher, C.J., *Computational Techniques for Fluid Dynamics*, Springer Series in Computational Physics, Springer-Verlag, Berlin Heidelberg, Germany, 2nd Edition, Vol. 1, (1991)

[11] Fletcher, C.J., *Computational Techniques for Fluid Dynamics*, Springer Series in Computational Physics, Springer-Verlag, Berlin Heidelberg, Germany, 1st Edition, Vol. 2, (1988)

[12] Abbot, M.B., and Basco, D.R., *CFD an Introduction for Engineers*, John Wiley and Sons, New York. (1989)

[13] Patankar, S.V., *Numerical Heat Transfer and Fluid Flow*, McGraw-Hill Book Company, (1980)

[14] Patankar, S.V., *Recent Developments in Computational Heat Transfer*, Jr. of Heat Transfer, Vol. 110, pp. 1037-1045, (1988)

[15] Patankar, S.V., *An Approach to Numerical Heat Transfer*, Proceedings of the 1978 Heat Transfer and Fluid Mechanics Institute at Washington State University, By Crowe, C.T. and Gross, W.L., pp. 143-145, (1978)

[16] Patankar, S.V., *Numerical Prediction of Three-Dimensional Flows*, Studies in Convection, By Launder, B.E., Academic Press London, pp. 1-78, (1975)

[17] Habib, M.A., *calculations of the Turbulent Flow and Heat Transfer in Expanding Duct*, 1989 ASME COGEN-TURBO, New York, 3rd International Symposium on Turbomachinery, Combined Cycle Technologies and Cogeneration, ASME, pp. 219-226, (1989)

[18] Bradshaw, P., *Effect of Streamline Curvature on Turbulent Flow*, AGARDograph 169, (1973)

[19] Pope, S.B., *The Calculation of Turbulent Recirculating Flows in General Orthogonal Coordinates*, Jr. of Computational Physics, Vol. 26, pp. 197-217, (1978)

[20] Habib, M.A., and Whitelaw, J.H., *The Calculation of Turbulent Flow in Wide-Angle Diffusers*, Num. Heat Transfer, Vol. 5, pp. 145-164, (1982)

[21] Shin, B.R., Ikohagi, T., and Daiguji, H., *A Finite-Difference Scheme for Two-Dimensional Incompressible Turbulent Flows Using Curvilinear Coordinates*, JSME Int. Jr., Series B, Vol. 36, No. 4, pp. 607-611, (1993)

[22] Benjamin, T.B., *Shearing Flows Over a Wavy Boundaries*, Jr. of Fluid Mechanics, Vol. 6, pp. 161-205, (1959)

[23] Gosman, A.D., *A Prediction Method for Fully-Developed Flow through Non-Circular Passages*, Numerical Methods in Laminar and Turbulent Flows, By Taylor, C., Morgan, K., and Brebbia, C.A., Swansea, U.K., July 1978, First International Conference, University of Swansea, Pentech Press, pp. 271-285, (1978)

[24] Asako, Y., and Faghri, M., *Finite-Volume Solution for Laminar Flow and Heat Transfer in a Corrugated Duct*, Jr. of Heat Transfer, Vol. 109, pp. 627-634, (1987)

[25] Faghri, M., and Asako, Y., *Numerical Determination of Heat Transfer and Pressure Drop Characteristics of Converging-Diverging Flow Channel*, ASME Jr. Heat Transfer, Vol. 109, pp. 606-612, (1987)

[26] Karol, Z.K., and Anthony, T.P., *An Isoparametric Spectral Element Method for Solution of Navier-Stokes Equation in Complex Geometry*, Jr. of Comp. Physics, Vol. 62, pp. 361-382, (1986)

[27] Shyy, W., Sun, C.S., Chen, M.H., and Chang, K.C., *Multigrid Computation for Turbulent recirculating Flows in Complex Geometries*, Num. Heat Transfer, Part A, Vol. 23, pp. 79-98, (1993)

[28] Gosman, A.D., Khalil, E.E., and Whitelaw, J.H., *The Calculation of Two-Dimensional Turbulent Recirculating Flows*, Turbulent Shear Flows 1, By Drust et al., Berlin Heidelberg, N.Y. 1979, First Int. Symposium on Turbulent Shear Flows, Penn. State University, Springer-Verlag, pp. 237-255, (1979)

[29] Amano, R.S., *A Numerical Study of Laminar and Turbulent Heat Transfer in a Periodically Corrugated Wall Channel*, Jr. Heat Transfer, Vol. 107, pp. 564-569, (1985)

[30] Chieng, C.C., and Launder, B.E., *On the Calculation of Turbulent Heat Transport Downstream from an Abrupt Pipe Expansion*, Trans. of ASME, HTD, Vol. 66, pp. 76-88, (1988)

[31] Amano, R.S., *A Study of Turbulent Flow Down-Stream of an Abrupt Pipe Expansion*, AIAA Jr., Vol. 21, No. 10, pp. 120-132, (1982)

[32] Hanratty, T.J., Abrams, J., and Frederic, K.A., *Flow Over Solid Wavy Surfaces*, Structure of Complex Turbulent Shear Flow, By Dumas, R., and Fulachier, L., IUTAM Symposium Marseille 1982, Springer-Verlag, pp. 79-88, (1983)

[33] Rodi, W., and Scheueree, G., *Scrutinizing the $k-\varepsilon$ Turbulence Model Under Adverse Pressure Gradient Conditions*, Trans. of ASME, Vol. 108, pp. 174-179, (1986)

[34] Elkaim, D., Reggio, M., and Camerero, R., *Simulating Two-Dimensional Turbulent Flow by Using $k-\varepsilon$ Model and the Vorticity-Stream Function Formulation*, Int. Jr. Num. Methods in Fluids, Vol. 14, pp. 961-980, (1992)

[35] Izumi, R., Yamashita, H., and Oyakawa, K., *Fluid Flow and Heat Transfer in Corrugated Wall Channels (4th Report. Analysis in the Case where Channels are Bent Many times)*, Bull. J.S.M.E., Vol. 26, No. 217, pp. 2098-2106, (1983)

[36] Amano, S., Bagherlee, A., Smith, R.J., and Niess, T.G., *Turbulent heat Transfer in Corrugated-Wall Channels with and without Fins*, Trans. of ASME, Vol. 109, pp. 62-67, (1983)

[37] Launder, B.E., and Spalding, D.B., *Lectures in Mathematical Models of Turbulence*, Academic Press Inc. (London) Ltd., (1972)

[38] Asako, Y., Nakamura, H., and Faghri, M., *Heat Transfer and Pressure Drop Characteristics in a Corrugated Duct with Round Corners*, Int. Jr. of Heat Mass Transfer, Vol. 31, No. 6, pp. 1237-1245, (1988)

[39] Zhu, J., *On the Higher-Order Bounded Discretization Scheme for Finite Volume Computations of Incompressible Flows*, Computer Methods in Applied Mechanics and Engg., Vol. 98, pp. 345-360, (1992)

[40] Kelkar, K.M., and Patankar, S.V., *Numerical Prediction of Flow and Heat Transfer in a Parallel Plate Channel with Staggered Fins*, Jr. of Heat Transfer, Vol. 109, pp. 25-30, (1987)

[41] Kelkar, K.M., and Patankar, S.V., *Numerical Prediction of Flow and Heat Transfer in a Longitudinal Fins Interrupted in Streamwise Direction*, Jr. of Heat Transfer, Vol. 112, No. 2, pp. 342-348, (1990)

[42] Webb, B.W., and Ramadhyani, S., *Conjugate Heat Transfer in a Channel with Staggered Ribs*, Int. Jr. Heat Mass Transfer, Vol. 28, No. 9, pp. 1679-1687, (1985)

[43] Ramadhyani, S., *Numerical Prediction of Flow and Heat Transfer in Corrugated Ducts*, Trans. of ASME, HTD, Vol. 66, pp. 37-43, (1986)

[44] Grag, V.K. and Maji, P.K., *Laminar Flow and Heat Transfer in a Periodically Converging-Diverging Channel*, Int. Jr. of Numerical Methods in Fluids, Vol. 8, pp. 579-597, (1988)

[45] Guzman, A.M., and Amon, C.H., *Flow Patterns and Force Convective Heat Transfer in Converging-Diverging Channels*, General Papers in Heat Transfer

Natural and Forced Convection, Trans. of ASME, HTD, Vol. 237, pp. 43-53, (1993)

[46] Amon, C.H., Majumdar, D., Herman, C.V., Mayinger, F., Mikic, B.B., and Sekalic, D.P., *Numerical and Experimental Studies of Self-Sustained Oscillatory Flows in Communicating Channels*, Int. Jr. of Heat Mass Transfer, Vol. 35, No. 11, pp. 3115-3129, (1992)

[47] Kang, I.S., and Chang, H.N., *The Effect of Turbulence Promoters on Mass Transfer - Numerical Analysis and Flow Visualization*, Int. Jr. Heat Mass Transfer, Vol. 25, No. 8, pp. 1167-1181, (1982)

[48] Wang, M., and Georgiadis, J.G., *Controlled Grid Generation on PC and Workstation for Fluid Flow*, Trans. of ASME, HTD, Vol. 185, pp. 67-74, (1991)

[49] Sparrow, E.M., and Hossfeld, L.M., *Effects of Rounding of Protruding Edges on Heat Transfer and Pressure Drop in a Duct*, Int. Jr. Heat Mass Transfer, Vol. 27, pp. 1715-1723, (1984)

[50] Sparrow, E.M., and Prata, A.T., *Numerical Solutions for Laminar Flow and Heat Transfer in a Periodically Converging-Diverging Tube with Experimental Confirmation*, Numerical Heat Transfer, Vol. 6, pp. 441-461, (1983)

[51] Patankar, S.V., Ramadhyani. S., and Sparrow, E.M., *Effect of Circumferentially Nonuniform Heating on Laminar Combined Convection in a Horizontal Tube*, Jr. of Heat Transfer, Vol. 100, pp. 63-69, (1978)

[52] Shuja, S.Z., *calculations of Fluid Flow and Heat Transfer in Expanding Ducts*, M.S Thesis, King Fahd University of Petroleum and Minerals, Dhahran, K.S.A, (1993)

[53] Ghaddar, N.K., Korczak, K.Z., Mikic, B.B., and Patera, A.T., *Numerical Investigation of Incompressible Flow in Grooved Channel*, Part 1. Stability and Self-Sustained Oscillations.

[54] Amon, C.H., and Patera. A.T., *Numerical Calculation of Stable Three-Dimensional Tertiary States in Grooved-Channel Flow*, Phys. Fluids. Part A, Vol. 1, No. 12, pp. 2005-2009, (1989)

[55] Izumi, R., *Fluid Flow and Heat Transfer in Corrugated Wall Channel(2nd Report, Experiments in the cases where channels are bent perpendicularly two times)*, Bull. J.S.M.E., Vol. 24, No. 198, pp. 2098-2106, (1981)

[56] Phan-Thien, N., and Khan, M.M.K., *Flow of an Oldroyd-Type Fluid Through a Sinusoidally corrugated Tube*, Jr. of Non-Newtonian Fluid Mechanics, Vol. 24, No. 2, pp. 203-220, (1987)

[57] Nishimura, T., Miyashita, H., Nurakami, S., and Kawamura, Y., *Effect of Strouhal Number on Flow Characteristics in a Symmetric Sinusoidal Wavy-Walled Channel for Oscillatory Flow*, Jr. of Chem. Engg. of Japan, Vol. 22, No. 5, pp. 505-511, (1989)

[58] Armaly, B.F., and Durst, F., *Reattachment Length and Circulation Regions Downstream of a Two-Dimensional Single Backward Facing Step.* Trans. of ASME, HTD, Vol. 64, pp. 1-8, (1986)

[59] Goldstein, L., and Sparrow, E.M., *Heat/Mass Transfer Characteristics for Flow in Corrugated Wall Channel*, Jr. of Heat transfer, Vol. 99, pp. 187-194, (1977)

[60] O'Brien, J.E., and Sparrow, E.M., *Corrugated Duct Heat Transfer, Pressure Drop and Flow Visualization.* Trans. of ASME, Vol. 104, pp. 410-418. (1982)

[61] Sparrow, E.M., and Comb, J.W., *Effect of Internal Spacing and Fluid Flow Inlet Condition on a Corrugated-Wall Heat Exchanger*, Int. Jr. of Heat Mass Transfer, Vol. 26, No. 7, pp. 993-1005, (1983)

[62] Oyakawa, K., Shinzato, T., and Mabuchi, I., *The Effects of the Channel Width on Heat Transfer Augmentation in a Sinusoidal-Wave Channel*, JSME Int. Jr., Series II, Vol. 32, No. 3, pp. 403-410, (1989)

[63] Zilker, D.P., Cook, G.W., and Hanratty, T.J., *Influence of the Amplitude of a Solid Wavy Wall on a Turbulent Flow*, Non-Separated Flows, Part 1. Jr. Fluid Mech., Vol. 82, pp. 29-51, (1977)

[64] Zilker, D.P., and Hanratty, T.J., *Influence of the Amplitude of a Solid Wavy Wall on a Turbulent Flow*, Separated Flows, Part 2, Jr. Fluid Mech.. Vol. 90, pp. 257-271, (1979)

[65] Greiner, M., Chen, R.F., nad Wirtz, R.A., *Enhanced Heat Transfer/Pressure Drop Measured from a Flat Surface in Grooved Channel*, Jr. of Heat Transfer, Vol. 113, pp. 498-501, (1991)

[66] Ektesabi, M.R.M, Sako, M., and Chiba, T., *Fluid Flow and Heat Transfer in Wavy Sinusoidal Channels (Part II. Pressure Drop and Flow Pattern of Turbulent Flow Field)*, Jr. of Fluid Mechanics, Vol. 47, No. 4, pp. 560-575, (1989)

[67] Sano, M., and Asako, Y.. *Fluid Flow and Heat Transfer in Periodically Diverging-Converging Turbulent Duct Flow*, JSME Int. Jr., Series B. Vol. 36, No. 2, pp. 207-213, (1993)

[68] Ali, M.M., and Ramadhyani, S., *Experiments on Convective Heat Transfer in Corrugated Channels*, Exp. Heat Transfer, Vol. 5, pp. 175-193, (1992)

[69] Molki, M., and Yuen, C.M., *Effects of Internal Spacing on Heat Transfer and Pressure Drop in a Corrugated-Wall Duct*, Int. Jr. Heat Mass Transfer. Vol. 29, pp. 987-997, (1986)

[70] Mendes, P.S., and Sparrow, E.M., *Periodically Converging-Diverging Tubes and their Turbulent Heat Transfer, Pressure Drop, Fluid Flow and Enhancement Characteristics*, Jr. of Heat Transfer, Vol. 106, pp. 55-63, (1984)

[71] Narayauan, C.M., and Bhattacharyya, B.C., *Some Studies on Heat Transfer in Diverging-Converging Geometries*, Ind. Engg. Chem. Research, Vol. 27, No. 1, pp. 149-153, (1988)

[72] Stephanoff, K.D., *Self-Excited Shear-Layer Oscillations in a Multi-cavity Channel with a Steady Mean Velocity*, Jr. of Fluid Engg., Vol 108, pp. 338-342, (1986)

[73] Nishimura, T., Ohori, Y., and Kawamura, Y., *Flow Characteristics in a Channel with Symmetric Wavy Wall for Steady Flow*, Jr. of Chemical Engg. of Japan, Vol. 17, No. 5, pp. 466-471, (1984)

[74] Nishimura, T., Ohori, Y., Kajimoto, Y., and Kawamura, Y., *Mass Transfer Characteristics in a Channel with Symmetric Wavy Wall for Steady Flow*, Jr. of Chemical Engg. of Japan, Vol. 18, No. 6, pp. 550-555, (1985)

[75] Nishimura, T., Kajimoto, Y., and Kawamura, Y., *Mass Transfer Enhancement in Channel with Symmetric Wavy Wall*, Jr. of Chemical Engg. of Japan, Vol. 19, No. 2, pp. 142-144, (1986)

[76] Nishimura, T., Kajimoto, Y., Tarumoto, A., and Kawamura, Y., *Flow Structure and Mass Transfer for a Wavy Channel in Transitional Flow Regime*, Jr. of Chemical Engg. of Japan, Vol. 19, No. 5, pp. 449-455, (1986)

[77] Nishimura, T., Murahami, S., and Kawamura, Y., *Flow Observations and mass Transfer Characteristics in Symmetrical Wavy-Walled Channels at Moderate Reynolds Number for Steady Flow*, Jr. of Chemical Engg. of Japan, Vol. 55, No. 5, pp. 505-511, (1989)

[78] Nishimura, T., Murakami, S., Arakawa, S., and Kawamura, Y., *Flow Observation and Mass Transfer Characteristics in Symmetrical Wavy-Walled Channels and Moderate Re No. for Steady Flow*, Int. Jr. of Heat Mass Transfer, Vol. 33, No. 5, pp. 835-845, (1990)

[79] Buckels, J., Hanaratty, T.J., and Adrian, R.J., *Turbulent flow over large amplitude wavy surfaces*, Jr. of Fluid Mechanics, Vol. 140, pp. 27-44, (1984)

[80] Saniei, N., and Dini, S., *Effects of Height and Geometry on Local Heat Transfer and Pressure Drop in Channel with Corrugated Walls*, Heat Transfer Engg., Vol. 14, No. 4, pp. 19-31, (1993)

[81] Thompson, J.F., *Numerical Grid Generation*, Proceedings of a Symposium on Numerical Generation of Curvilinear Coordinate System and their use in Numerical Solution of PDE, April 1982, Nashville Tenesse, North Holland. (1982)

[82] Patankar, S.V., *Computer Analysis of Fluid Flow and Heat Transfer*, Computational Techniques in Transient and Turbulent Flow, By Taylor, C., and Morgan, K., Chap. 8, Pineridge Press Ltd, Swansea U.K., pp. 223-252, (1981)

[83] Chen, H.C., and Patel, V.C., *Near-Wall Turbulence Models for Complex Flows Including Separation*, AiAA Jr., Vol. 26, pp. 641-648, (198)

[84] Habib, M.A., Attya, A.E., and McEligot, D.M., *Calculation of Turbulent Flow and Heat Transfer in Channel with Streamwise-Periodic Flow*, Jr. of Turbomachinery, Vol. 110, No.3, pp. 405-411, (1988)

[85] Yang, B.T., and Yu, M.H., *The Flow Field in a Suddenly Enlarged Combustion Chamber*, AIAA Jr., Vol. 21, No. 1, pp. 92-97, (1983)

[86] Ota, T., and Nishiyama, H., *Turbulent Heat Transfer at the Reattachment Point of Separated Flows*, Prepr. of 21st Symp. Heat Transfer Soc. Japan, pp. 112-120, (1984)

[87] Durao, D.F.G., Heitor, M.V., and Moreira, A.L.N., *The Turbulent Characteristics of the Swirling Flow in Typical Burners*, Engg. Turbulence Modelling and Experiments. By Rodi, W., and Ganic, E.N., Proceedings of the Interna-

tional Symposium on Engineering Turbulence Modelling and Measurements, Dubrovnik, Yogoslavia, pp. 705-716, (1990)

[88] Gupta, A.K., Lilley, D.G., and Syred, N., *Swirl Flows*, Energy and Engineering Science Series, Abacus Press, Kent, England, (1984)

[89] Hallett, W.L.H., and Gunther, R., *Flow and Mixing in Swirling Flow in a Sudden Expansion*, Canadian Jr. of Chem. Engg., Vol. 62, pp. 149-155, (1984)

Vitae

- Ikram-Ul-Haq
- Born on October 15th 1968 in Karachi, Pakistan
- Received Bachelor of Engineering (**B.E**) degree in Mechanical Engineering from **NED** University of Engineering and Technology, Karachi, Pakistan in April 1993
- Joined the Department of Mechanical Engineering at King Fahd University of Petroleum and Minerals (**KFUPM**), Dhahran, Saudi Arabia as a Research in January 1993
- Received Master of Science (**M.S**) degree in Mechanical Engineering from KFUPM, Saudi Arabia in May 1995